SYNTHESIS AND CHARACTERIZATION OF IRON DOPED HYDROXYAPATITE FOR DEFLUORIDATION OF WATER

ABEBE AWULEW TEMTIME

A THESIS SUBMITTED TO THE DEPARTMENT OF APPLIED CHEMISTRY,

SCHOOL OF APPLIED NATURAL SCIENCE

PRESENTED IN PARTIAL FULFILLMENT OF THE REQUIREMENT FOR THE DEGREE OF MASTER'S IN INORGANIC CHEMISTRY

OFFICE OF GRADUATE STUDIES

ADAMA SCIENCE AND TECHNOLOGY UNIVERSITY

November, 2022

Adama, Ethiopia

SYNTHESIS AND CHARACTERIZATION OF IRON DOPED HYDROXYAPATITE FOR DEFLUORIDATION OF WATER

ABEBE AWULEW TEMTIME

ADVISOR: DR. ENYEW AMARE ZEREFA

CO-ADVISOR: DR. DEREJE TSEGAYE LEKU

A THESIS SUBMITTED TO THE DEPARTMENT OF APPLIED CHEMISTRY,

SCHOOL OF APPLIED NATURAL SCIENCE

PRESENTED IN PARTIAL FULFILLMENT OF THE REQUIREMENT FOR THE DEGREE OF MASTER'S IN INORGANIC CHEMISTRY

OFFICE OF GRADUATE STUDIES

ADAMA SCIENCE AND TECHNOLOGY UNIVERSITY

November, 2022

Adama, Ethiopia

Declaration

I hereby declare that this Master Thesis entitled “Synthesis and Characterization of Iron Doped Hydroxyapatite for Defluoridation of Water” is my original work. That is, it has not been submitted for degree in any other university. An original research work carried out by me under the guidance and supervision of Dr. Enyew Amare and Dr. Dereje Tsegaye, Department of Applied Chemistry, Adama Science and Technology University. All sources of materials that are used for this thesis have been duly acknowledged through citation.

_____	_____	_____
Name of student	Signature	Date

Recommendation of Advisors

We, the advisors of this thesis, hereby certify that we have read the revised version of the thesis entitled “Synthesis and Characterization of Iron Doped Hydroxyapatite for Defluoridation of Water” prepared under our guidance by Abebe Awulew Temtime submitted in partial fulfillment of the requirements for the degree of Mater’s of Science in inorganic chemistry. Therefore, we recommend the submission of revised version of the thesis to the department following the applicable procedures.

_____	_____	_____
Major Advisor	Signature	Date
_____	_____	_____
Co-advisor	Signature	Date

Approval Page

We, the advisors of the thesis entitled "Synthesis and Characterization of Iron Doped Hydroxyapatite for Defluoridation of Water" and developed by Abebe Awulew; hereby certify that the recommendation and suggestions made by the board of examiners are appropriately incorporated into the final version of the thesis.

Major Advisor	Signature	Date
Co-advisor	Signature	Date

We, the undersigned, members of the Board of Examiners of the thesis by Abebe Awulew have read and evaluated the thesis entitled "Synthesis and Characterization of Iron Doped Hydroxyapatite for Defluoridation of Water" and examined the candidate during open defense. This is, therefore, to certify that the thesis is accepted for partial fulfillment of the requirement of the degree of Master of Science in Inorganic chemistry.

Chairperson	Signature	Date
Internal Examiner	Signature	Date
External Examiner	Signature	Date

Final approval and acceptance of the thesis is contingent upon submission of its final copy to the Office of Postgraduate Studies through the Department Graduate Council and School Graduate Committee.

Department Head	Signature	Date
School Dean	Signature	Date
Office of Postgraduate Studies, Dean	Signature	Date

ACKNOWLEDGEMENT

First of all, I would like to thank my God for being with me in all aspects of my work. He helped me by his wisdom, knowledge, understanding, and kindness and gave me the health and strength to complete this thesis. Next, I would like to thank my advisor Dr. Enyew Amare for his cooperation, suggestions, supervision and guide, and taking his time to read and correct my documents, starting from the proposal writing to the completion of this thesis. Next, I would like to thank my Co-Advisor Dr. Dereje Tsegaye for his advice and guidance me by all his knowledge starting from the beginning to the end of my thesis work with his continuous help. I would like to thank Oromia Self-Help Organization Fluoride Removal Technology Center for helping me to do fluoride removal work in their laboratory, and I would like to thank Adama Public Health Research and Referral Laboratory for helping me to do antibacterial activity investigation in their laboratory. Also, I would like to thank chemistry and biology academic and research assistants for helping me by giving apparatus and some chemicals that I needed for my work. Finally, I would like to thank all my family and my friends who helped me in all direction for my success through the difficult times.

Table of Contents

Contents **Page**

LIST OF TABLES

LIST OF FIGURES

LIST OF ABBREVIATIONS

ASTU	Adama science and technology university
AMX	Amoxicillin
Ca/P	Calcium to phosphate ratio
CTAB	Cetyltrimethylammonium bromide
DAP	Di-ammonium hydrogen phosphate
DMSO	Dimethyl sulfoxide
DTA	Differential thermal analysis
FISE	Fluoride ion selective electrode
FTIR	Fourier transformer infrared
HAp	Hydroxyapatite
JCPDS	Joint committee on powder diffraction standards
PHpzc	pH at point of zero charge
PLA	polylactic acid
SEM	Scanning electron microscopy
TCP	Tri-calcium phosphate
TGA	Thermogravimetric analysis
TISAB	Total ionic strength adjustment buffer
WHO	World health organization
XRD	X-ray diffraction

ABSTRACT

According to the World Health Organization the maximum acceptable concentration of fluoride ions in drinking water lies below 1.5 mg/L. Fluoride if taken in small amount is usually beneficial, but the beneficial fluoride concentration range for human health is very small. For this reason the development of materials for the removal of fluoride from aqueous solution is in progress. This study was focused on the synthesis of Iron doped hydroxyapatite (Fe-HAp) from diammonium hydrogen phosphate (DAP), Calcium and Iron precursors using urea as fuel for defluoridation of water and antibacterial activities. The synthesized pure hydroxyapatite (HAp) and Fe-HAp were characterized by using thermogravimetric analysis; scanning electron microscopy, X-ray diffraction, and Fourier transform Infrared spectroscopic techniques. Average crystallite size of HAp and Fe-HAp were 32.54 nm and 27.91 nm, respectively. Batch experiments were performed to investigate the adsorption capacity of Fe-HAp such as the initial pH of the solution, contact time, adsorbent dose and initial fluoride concentration. Accordingly, the optimum adsorption capacity was observed at pH 3, contact time 3 hr, adsorbent dose 0.7 g, and initial fluoride concentration of 10 mg/L. The correlation coefficients of Langmuir isotherm (R^2 = 0.9796) and the Freundlich isotherm (R^2 = 0.9968) kinetic studies, show that adsorption was fitted with Freundlich isotherm model. Also the correlation coefficients of pseudo first order (R^2 = 0.874) and pseudo second order (R^2 = 0.9969), show that the adsorption was fitted with pseudo second order kinetic model. The maximum fluoride removal efficiency of synthetic water and groundwater obtained by using the material developed, Fe-HAp, to be 98 % and 82.9 %, respectively, under the optimum conditions. The maximum adsorption capacity of synthesized Fe-HAp was 4.2 mg/g. The antibacterial activities of the synthesized HAp_4 and $Fe_{0.05}HAp$ tested against gram-negative bacterial strains E. coli by disc diffusion method was about 11 mm for both HAp_4 and $Fe_{0.05}HAp$. The maximum inhibition zone of gram-positive bacterial S. aureus was found to be 8 mm for HAp_4 and $Fe_{0.05}HAp$.

Keywords: *Hydroxyapatite, Fe -HAp, Antibacterial activity, Defluoridation, Adsorbent*

1. INTRODUCTION

1.1. Background of the Study

Water is a very essential natural resource for life. The dissolved minerals are leached into water and accumulated into ground water sources and other water bodies. Water bodies have mineral elements that are found within a particular locality dissolved in different concentrations as a result of the geological composition of soils and bedrock. Fluorite (CaF_2), sellaite (MgF_2), Fluorapatite (Ca_5 $(PO_4)_3F$), cryolite (Na_3AlF_6) and topaz (Al_2SiO_4 $(F, OH)_2$) are the most common fluoride bearing minerals (Mukherjee & Singh, 2020). These natural sources of fluoride are breakdown and leach the fluoride ions. The other major sources are the run offs from the agricultural fields (fertilizer) treated with insecticides and pesticides containing fluorides that come from unplanned and uncontrolled discharge from the industrial wastes are primarily responsible for fluoride contamination (Kanrar et al., 2016). Fluorides are released into the environment naturally through weathering and dissolution of rock minerals, in releases of volcanoes, and in marine aerosols. The major source of fluoride ions that pollute water is the natural weathering process (Ayoob et al., 2008).

Fluoride contamination has become a major geo-environmental concern in many parts of the world particularly in developing countries such as Kenya, Egypt, Ethiopia, India, South Africa, Argentina and Australia. Fluoride in groundwater exists at different concentrations ranging from less than 1 in highly elevated highlands to as high as 200 mg/L in the central Ethiopian rift (Ayenew, 2008). Study along Hawassa and Ziway area reported levels of fluoride of up to 13.2 and 7.5 mg/L of ground water respectively (Akafu et al., 2019). Study along Meki area reported levels of fluoride of up to 10.5 mg/L ground water (Workeneh et al., 2019). Study along Raebareli District in India reported levels of fluoride of up to 4.2 mg/L of ground water (Kanaujia et al., 2015). Study along South Africa reported levels of fluoride of up to 5.53 mg/L of ground water (Izuagie et al., 2016). Study along Kenya Gilgil Elementaita reported levels of fluoride of up to 200 mg/L in Lake Water, 7.69 mg/L in piped water and 6.57 mg/L in borehole water (Wambu & Muthakia, 2011).

The fluoride concentrations measured and reported in many areas are higher than that described by the World health organization (WHO). The maximum limit of fluoride in drinking water is 1.5 mg/L according to the Standards of WHO. Excessive intake of fluoride ions (>1.5 mg/L) can lead to various diseases such as fluorosis, cancer, infertility, brain damage, osteoporosis, arthritis, brittle bones, thyroid disorder, and Alzheimer syndrome (Dhillon et al., 2015). High concentration of fluoride ion in water leads to decrease in dissolved calcium and magnesium ions in water. It also affects the skeletal and dental fluorosis. This causes mineralization of the teeth and bones leading to dental and skeletal fluorosis respectively (Bhatnagar & Minocha, 2006). Dental fluorosis may be of varying degree depending on structural damage of the enamel layer. If the enamel is highly damaged, it may be more than a cosmetic damage. In such a case it's going to end in pain. This adversely affects food choices, compromises the rate of chewing and may require complex dental treatment. Skeletal fluorosis with adverse change in bone structure may be observed when water contains 3–6 mg/L of fluoride. Fluorosis is an irreversible condition and the only medicine is prevention by keeping the fluoride levels in drinking water within the safe limits (Rajan & Alagumuthu, 2013). East African Rift Valley is one among the regions in the world highly affected by fluorosis. This is due to presence of fluorotic minerals from the volcanic rocks which often contaminate the ground water and later the adjacent water bodies with the fluoride ions. In Kenya for example regions along the Great Rift Valley and at the slopes of Mount Kenya have been reported to have high fluoride levels. At the Rift Valley region of Ethiopia have well documented cases of dental fluorosis and skeletal fluorosis (Ayenew et al., 2008).

The above mentioned researches reported summarized about the level of fluoride concentration above WHO standard limit and its effect on human health. In order to prevent health hazards fluoride ion need to be removed from water using various methods. The methods available for defluoridation of water include precipitation method, membrane method, ion exchange method, and adsorption method. The adsorption method is considered more appropriate for defluoridation due to its simplicity, effectiveness, and economic viability (Ali & Gupta, 2007). Adsorption process is affected by pH of the solution, initial concentration, contact time and adsorbent dosage. The commonly used instrument for measuring of fluoride ion concentration in water samples is fluoride ion selective electrode (FISE). All FISE have a common feature in their design in that the ion sensing parts consist of a membrane.

The advantages of fluoride ion selective electrode method are easy operation, simple equipment, good selectivity, and high accuracy, and wide measurement concentration range 0.05–1900 mg/L (Wang et al., 2019). Recently, several researchers have investigated a range of calcium-based adsorbent materials, of which synthesis hydroxyapatite (HAp) has been the promising candidate due to its identical chemical composition with bone, nontoxicity, and specifically high fluoride removal capability (Mehta et al., 2016; Kanno et al., 2014; Sundaram et al., 2008; Xia et al., 2018; Workeneh et al., 2019). Review results indicated that HAp has better defluoridation capability adsorbent material (Maity et al., 2018).

HAp was prepared by different methods such as precipitation methods, sol-gel method, hydrothermal method, combustion method, pyrolysis method and solid state method. Among these, combustion method is used for this research. Combustion method is inexpensive in raw materials, relatively simple preparation process, and well chemical homogeneity of synthesized powder as a result of intimate blending of constituents (Ghosh et al., 2011). When combustion method used, there is a quick exothermic reaction takes place and delivering high amount of energy and promotes wide thermal gaps. In order to decrease high amount of energy and promotes narrow thermal gaps use urea as fuel. HAp can be synthesized from egg shell, fish scale, fish bone, bovine bone, calcium and phosphate source precursors and organic fuel (Ismail et al., 2019, P. Shi et al., 2018, (Malla et al., 2020), Han et al., 2004). In this study HAp can synthesis from iron, calcium and phosphate source precursors and urea. The synthesized Fe doped HAp (Fe-HAp) improves both their stability and biocompatibility. Fe-HAp could be employed as a feasible new adsorbent material for industrial waste water and groundwater treatment. Fe is considered as a dopant in HAp, because it is, potentially less toxic than other transition metals (Hadagalli et al., 2021).

HAp has an ability to inhibit the growth of bacterial activity. Drinkable water is often contaminated with microbes for instance; *Escherichia coli (E. coli).* The presence of *E. coli* in water is a strong indication of current animal waste impurity. For instance, during rainfall and snow melt, *E. coli* could also be washed into creeks, rivers, streams, lakes, or groundwater from the land surface. Harmful strains of *E. coli* ingested in human body by various means can cause diarrhea, vomiting, severe anemia, kidney failure, urinary tract infections, and other infections.

The different mass fractions of Fe-HAp nanoparticles mixed with polymeric matrix of polylactic acid (PLA) nanocomposites showed a high inhibitory effect of antibacterial activity against *E.coli* bacteria and *Staphylococcus aureus (S.aureus)* bacteria (Morsi & Hezma, 2019). The PLA-Fe-HAp nanoparticles nanocomposites had high antibacterial activity than pure PLA. The Fe-HAp nanoparticles mixed with polymeric matrix of polylactic acid nanocomposites could be tailored for many biomedical applications. Different concentrations of Fe-HAp powder was mixed with amoxicillin (AMX) powder in the ratio of 1: 0.5 (100 mg of Fe-HAp to 50 mg of AMX) showed a good inhibitory effect against gram negative bacteria E. coli reported by (Jose et al., 2021). The aim of this study work was to synthesis high purity HAp and Fe-HAp using urea as fuel and investigates their efficacy for defluoridation of water and antibacterial activity.

1.2. Statement of the Problem

Ground water is one of major the source for drinking water supply in rural communities in developing countries. Problems can, however, arise with the chemistry of groundwater and make it unsafe, due to elevated concentrations of some elements that can have negative health impacts on the user. Fluoride is one of the water quality parameters of concern, but the excess of which contaminates groundwater resources in many parts of the world, and renders it not drinkable for human ingestion, due to the related adverse health effects. There is the negative health impact of excess fluoride in drinking water; however, the search for an appropriate technology for its removal from polluted groundwater still remains very critical. The second problem is increment of bacterial infectious diseases. The bacteria *E. coli* present in drinking water can cause diarrhea, vomiting, headaches, and kidney failure. The prime preventable challenge for healing wounds is a topical infection by bacteria. Therefore, to solve this problem utilization of an appropriate removal technique, high fluoride removal capability and good antibacterial material is crucial. Calcium-based, HAp materials, has been the promising candidate due to its identical chemical composition with bone, nontoxicity, and specifically high fluoride removal and antibacterial capability. In this study iron modified hydroxyapatite was synthesized by optimization mole of Fe by combustion method for defluoridation of water and antibacterial activity by disc diffusion method.

1.3. Objectives of the Study

1.3.1. General Objective

The general objective of this study was to synthesis Fe-HAp for defluoridation of water and antibacterial activity.

1.3.2. Specific objectives

i. To synthesis HAp and Fe-HAp powder from iron nitrate nonahydrate, calcium nitrate tetrahydrate, diammonium hydrogen phosphate, concentrated nitric acid and urea.

ii. To characterize the synthesized HAp and Fe-HAp powder using Thermogravimetric analysis, Scanning electron microscopy, Fourier transformer infrared and X-ray diffraction.

iii. To test the synthesized Fe-HAp powder for fluoride removal from ground water.

iv. To test the synthesized HAp and Fe-HAp powder against *Escherichia coli* and *Staphylococcus aureus* bacteria.

1.4. Significance of the Study

This study provides information about defluoridation efficiency of HAp and Fe-HAp powder and its antibacterial activity. The use of synthesis of Fe-HAp is expected to improve availability of free water from fluoride ion for communities.

1.5. Scope and Limitations of the Study

This study was limited to the synthesis of HAp and Fe-HAp using urea as fuel by combustion method, evaluation of its effectiveness on the test of fluoride removal from water by adsorption method and investigate of antibacterial activity against gram-negative bacteria *E. coli* and against gram-positive bacteria *S. aureus* by disc diffusion method, and the synthesized HAp and Fe-HAp powder were characterized using Thermo gravimetric analysis, Scanning electron microscopy, Fourier transformer infrared and X-ray diffraction techniques.

2. LITERATURE REVIEW

2.1. Hydroxyapatite

The term "apatite" applies to a group of compounds (not only at calcium phosphates) with a general formula in the form $M_{10}(XO_4)_6Z_2$, where M^{2+} may be a metal and species XO_4^{3-} and Z^- are anions. The particular name of every apatite depends on the elements or radicals M, X and Z. In these terms, hydroxyapatite has the molecular structure of apatite, where M is calcium (Ca^{2+}), X is phosphate (PO_4^{3-}) and Z is the hydroxyl radical (OH). Hydroxyapatite is chemically related to inorganic component of bone matrix as a complex structure with formula ($Ca_{10}(PO_4)_6(OH)_2$). It is recognized as stoichiometric HAp (ratio of Ca/P =1.67) and written as $Ca_{10}(PO_4)_6(OH)_2$, containing 3.38% of OH, 18.5% P, and 39% of Ca by weight. Empirical formula of hydroxyapatite can be written as $Ca_5(PO_4)_3OH$. Synthetic HAp is similar to the inorganic component of natural bone; vast differences exist with respect to the total chemical composition, stoichiometry and structure (Zaman et al., 2020).

2.2. Metal Doped Hydroxyapatite (M-HAp)

HAp have two different binding sites on the crystal surface, one is Ca^{2+} site and other PO_4^{3-} site. Besides, due to its higher binding sites abundant cationic substitution can be created. In HAp structure, cationic and anionic doping and substitutions are possible to a greater extent. Recent studies reported that Ca^{2+} cationic sites can be replaced by various transition metals which modify the functionality of HAp (Fakharzadeh et al., 2017). Several transition metals (Fe, Ru, Mn, etc.,) have doped at Ca site in HAp to create antibacterial property and to increase electronic/ionic conductivity of HAp (Singh et al., 2018). Iron is one of transition metal that doped/substituted at Ca site in HAp and to increase the application of HAp. The Fe^{3+} ionic substitution into HAp ($Ca_{10-x}Fe_x(PO_4)_6(OH)_2$) can improve the removal efficiency of fluoride and bactericidal. The crystallinity decreases with the increase of magnetic ion incorporation. When Iron add to HAp, Carbon dioxide was brought in which could cause significant reduction of HAp size and morphological changes. The Fe-HAp results suggest that the Fe doping concentrations has its physical effects in decreasing the particle size along with remarkable changes in its increased hardness and dielectric properties of HAp. Similarly, Fe-HAp drug release analysis indicates that the dopant is effective for extended drug release characteristics.

The porous structure of hexagonal Fe-HAp is used for fluoride removal from water, in the areas of catalysis, drug delivery, and biomolecules sorption. The existence of magnetic ions leads to the formation of superparamagnetic porous structures composed of hexagonal HAp (Ma et al., 2019). The usage of superparamagnetic Fe-HAp nanoparticles for biological and medical purposes has been increasing. Fe-HAp is an excellent applicant for effective dye removal agent and could be useful in industrial waste water treatment (Panneerselvam et al., 2019).

2.3. Synthesis Method of HAp

In order to get good morphology, uniform composition, small particle size, large specific surface area, fine grain and high crystallite size of HAp, researchers have been used different synthesis method. Commonly methods are hydrothermal method (Méndez-lozano et al., 2016), precipitation method (Cahyaningrum et al., 2018), sol- gel method (Chitra et al., 2020), combustion method (Batista et al., 2020), micro-emulsion method (Koumoulidis et al., 2003), ultrasonic synthesis method (Cao et al., 2005), microwave irradiation method (Govindaraj & Rajan, 2016) and solid state method (Pramanik et al., 2007). Among them, the most widely used, the low cost and the best HAp comprehensive properties obtained by scientific research workers in recent years are hydrothermal method, sol-gel method, combustion method and precipitation method (Ma et al., 2019).

2.3.1. Hydrothermal Method

The hydrothermal process is a wet chemical technique able to direct the formation of complex oxide powders with high crystallinity, making it the most popular method used to prepare hydroxyapatite nanoparticles. Hydrothermal processes usually work with a chemical reaction in an aqueous solution at high temperature and pressure. Due to its high biocompatibility, this has become a favored technique for material production (Zhu et al., 2006). In recent years, hydrothermal preparation of hydroxyapatite has become increasingly mature. Studies have found that the shape and size of hydroxyapatite can be regulated by changing the hydrothermal temperature, hydrothermal time and reaction concentration. According to this method, researchers have prepared high purity hydroxyapatite of different shapes, such as nano spherical, rod-like, needle-like, flake, hexagonal prism, small plate and spine-like (Wu et al., 2015). Synthesis hydroxyapatite nano-rod like particles from cetyltrimethylammonium bromide (CTAB) was reported by (Hoai et al., 2017).

Nanosized HAp rods with composition resembling that of bone minerals could be obtained when using a suitable amount of CTAB and hydrothermal duration. HAp nanorod can prepare from phosphogypsum waste and potassium dihydrogen phosphate (Bensalah et al., 2018). The microporous synthesized hydroxyapatite crystals from calcium nitrate and phosphorus oxide was reported by (Xu et al., 2011). HAp whisker was prepared with good crystallization, uniform structure and high aspect ratio by using acetamide as raw material (Zhang & Darvell, 2011).

The pH value of the system has a great influence on the growth of HAp crystal. With the increase of pH value, HAp particle size and length-width ratio decreased significantly. Increasing hydrothermal temperature and prolonging hydrothermal time can significantly increase the crystallinity of HAp and increase the size of HAp. The advantage of hydrothermal method is the highly crystalline and no hydroxyl defects are produced in the structure. The disadvantage of hydrothermal method is poor capability to control the morphology and size of HAp nanoparticles.

2.3.2. Sol – Gel Method

Sol-gel method a chemical route used to synthesize glassy or ceramic materials ceramic materials at relatively low temperatures, based on wet chemistry processing, that involve the preparation of a sol, the gelation of the sol and the removal of the liquid existing in fine interconnected channels within the gel. This method uses the reaction of calcium citrate or calcium acetate with phosphoric acid to obtain sol, and the sol is aged into gel under certain conditions. The gel is dried at low temperature and calcined at high temperature under vacuum to obtain nanometer hydroxyapatite. Some study found that the condition changes such as the initial concentration of the solution, reaction atmosphere and mole ratio of calcium and phosphate, hydrolysis time, add way and speed, aging time, the gel treatment method, calcination temperature (Zhou & Lee, 2011).

The all condition changes have more or less impact on crystal morphology, crystallization degree and performance of the obtained HAp powder. By changing raw materials, relevant parameters and processes, HAp powders with good uniformity, high purity, fine particle size, various morphology, good crystallinity and high surface activity can be prepared under different conditions.

The basicity and temperature of sol heat treatment and other synthesis conditions in order to control the growth, evolution and purity of HAp nanoparticles when Ca $(NO_3)_2.4H_2O$ and P_2O_5 are used to synthesize nano and sub-micron monodisperse HAp particles (Dardouri et al., 2017). The microcrystalline synthesized HAp powders from calcium acetate and triethyl phosphate in water and ethanol medium was reported by (Vijayalakshmi & Rajeswari, 2006). The advantages of sol-gel method are the lattice is relatively complete, high purity, low processing temperature and can be used to prepare nano composite materials. The disadvantages of sol-gel method are chemical process is complex, crystallinity and sintering property is poor, preparation cost is high and environment, and easy agglomeration during calcination.

2.3.3. Precipitation Method

The chemical precipitation method is one of the broadest research techniques used for synthesizing HAp. This method is widely used since a large amount of HAp can be synthesized at a reasonable cost (Santos et al., 2004). The most commonly used technique for the formation of HAp is the precipitation, which involves wet chemical reactions between the calcium and phosphate precursors under controlled temperature and pH conditions.

In order to form precursor precipitate, namely colloidal HAp precipitation, certain pH, temperature and solution conditions are often required. The Calcium hydroxide (Ca $(OH)_2$) and orthophosphoric acid (H_3PO_4) were starting materials (Equation 1) for synthesis of HAp was proposed by (Bouyer et al., 2000).

$$10\ Ca(OH)_2 + 6\ H_3PO_4 \rightarrow Ca_{10}(PO_4)_6(OH)_2 + 18\ H_2O \quad \text{.....(1)}$$

The size, shape and surface area of the HAp particles obtained by this reaction are very sensitive to the H_3PO_4 addition rate and the reaction temperature. The H_3PO_4 addition rate is strongly linked to the pH obtained at the end of the synthesis, and also to the suspension stabilization. The advantages of precipitation method are: simple technology, low reaction temperature, low cost, simple operation, small product particles, can produce nano HAp particles and high purity. The disadvantages of precipitation method are: have a poor uniformity, agglomerated, difficulty to control of the pH value over 9 to avoid the formation of a Ca-deficient HAp.

2.3.4. Combustion Method

The basis of combustion method comes from thermo-chemical concepts used in the field of propellants and explosives chemistry. Combustion synthesis is a two-step process: formation of precursor and then auto ignition. This auto-ignition is often termed as self-propagating high temperature synthesis. The combustion method uses rapid exothermic and self-sustaining redox reactions between the oxidant and organic fuel in an aqueous phase (Sadat-Shojai et al., 2013). The combustion of metal nitrates urea mixtures in water solution usually occur as a self-propagating and non-explosive exothermic reaction. Water soluble nitrate salts of the desired metal ions and urea are the most common starting materials for the solution combustion processing. Metal nitrates are the preferred salts because they are soluble in water whereby better mixing is achieved and uniformity of the product results.

The stoichiometric glycine calcium nitrate leads to the higher flame temperature compared to stoichiometric urea calcium nitrate system, resulting in a powder with lower specific surface area. Moreover, in both cases of glycine and urea, combustion with excess fuel produced particles with higher surface area. The feasibility of producing nanocrystalline particles and the thermal behavior of HAp during synthesis with regard to initial Ca/P atom ratio in the solutions is also investigated. Also demonstrated that a decrease in both batch size and initial furnace temperature and an increase in fuel to oxidizer ratio result in a decrease in crystallite size reported by (Ghosh et al., 2010). The advantages of combustion method are inexpensive raw materials, relatively simple preparation process, and well chemical homogeneity of synthesized powder as a result of intimate blending of constituents. The disadvantages of combustion method are aggregation can occur, low crystallinity and at high temperature HAp decompose into α-TCP.

2.4. Applications of HAp

Synthesis HAp is mostly used in biomedical applications; these bridging agents must fulfill certain requirements. Hence, (i) they should not compromise the biocompatibility, (ii) they should not be cytotoxic, and (iii) they should not alter the physiological or biological properties of the HAp or fillers (Haider et al., 2017). HAp is widely used in biomedical applications for hard tissue repair, drug delivery systems, dental fillers, bone fillers or Bone Grafts, coating implants, and bone substitutes for bone reconstruction and regeneration, due to their chemical similarity to the mineral component of hard tissue (Sobczak-Kupiec et al., 2021).

From the point of view of biocompatibility; HAp seems to be the most appropriate choice for hard tissue replacement implants. It shows excellent biocompatibility with hard tissues and also with skin and muscle tissues. HAp powder and granules have been used for bone grafting and augmentation while dense as well as porous blocks have found application as implant material in the field of dentistry and orthopaedics. When HAp nanocrystal is used as a bone substitute graft, rapid healing of critical size defect has been demonstrated in animal experiments and applications in humans. HAp nanocrystal will be bound to the bone and stimulate bone healing through the stimulation of osteoblast activity. Small amounts of iron were found to have the positive impact on the biomedical properties of HAp (Panseri et al., 2012). The Fe-HAp had the positive effects on the osteoblast viability and they could be used for diagnostic imaging or drug delivery. The addition of Fe^{3+} ions in HAp enhanced the osteoblast adhesion and Fe-HAp samples had no toxic effect on the osteoblast cells (Li et al., 2012). Also synthesis HAp used for antibacterial activity, because of HAp has an ability to inhibit bacteria growth. This study focused on the removal of fluoride ion from water and antibacterial activity.

2.4.1. Antibacterial Activity

HAp has excellent bioactivity and biocompatibility along with strong antibacterial activity. The HAp nanoparticles has higher antibacterial efficacy towards E.coli bacteria. It is clear that treatment of the E. coli bacteria with HAp nanoparticles had led to considerable damage to E. coli which caused the breakdown of the bacterial cell wall. The OH^- presence on HAp surface can inhibition a cell wall of bacteria (Ragab et al., 2014). The replacing of Ca^{2+} ions with Fe^{3+} can improve the antibacterial activity performance of HAp. The antibacterial activity test of Fe-HAp mixed with amoxicillin antibiotic displays inhibition to the bacterial strains. The studies on the antibacterial efficiency of AMX loaded Fe-HAp samples were analyzed against *E.coli* bacteria by the disk diffusion method. Different concentrations of Fe-HAp powder was mixed with amoxicillin powder and used for antibacterial activity. AMX loaded Fe-HAp samples showed good inhibitory effect against *E. coli* (Jose et al., 2021).

2.4.2. Defluoridation of Water

HAp is a member of the calcium phosphate family with high biocompatibility and essentially no toxicity, which has been used as an adsorbent for efficient and selective removal of fluoride from water.

It can remove fluoride through adsorption and ion exchange to form thermodynamically more stable fluorapatite ($Ca_5(PO_4)_3F$), or mixed fluoridated HAp ($Ca_5(PO_4)_3(OH, F)$)(He et al., 2016). The commonly used instrument for measuring fluoride ion concentration in water samples is FISE. All FISE have a common feature in their design in that the ion sensing part contain of a membrane (Radu et al., 2013). The advantage of FISE instrument is easy operation, simple equipment, good selectivity, and high accuracy, small influence on water sample turbidity and chromaticity, and wide measurement concentration range (0.05–1900 mg/L) (Wang et al., 2019).

2.5. Common Fluoride Removal Methods

Removal of fluoride ions from water is important for environmental conservation and human health. The main methods utilized in defluoridation of water include: electro dialysis, reverse osmosis, ion exchange, chemical precipitation and adsorption. The method chosen in removal of fluoride depends on factors such as capital and operational cost, effect on the environment and effectiveness in fluoride removal of the method.

2.5.1. Electro dialysis Method

Electro-dialysis is the removal of ionic components from aqueous solutions through ion exchange membranes under the driving force of an electric. It consists of a series of cation and anion exchange membranes which are arranged between the cathode and the anode. The cation migrate to the cathode while anions to the anode. These ions permeate through the membrane and are retained by the oppositely charged electrodes. (Ergun et al., 2008) used electro dialysis with anion exchanger membrane for removal of fluoride from water having 20.6 mg/l of fluoride and decrease it to 0.8 mg/l suitable for drinking purpose in spite of the presence of chloride and sulphate ions. The advantage of this method is that it is inexpensive post treatment, flexible, low chemical request and high water recovery. The limitations of this method is that it is only separation of ionic components, potential formation of H_2 in the electrode rinse, specific power consumption for pumping and necessity of concentrate treatment.

2.5.2. Ion-Exchange Method

Ion exchange is a process where the ion removed from aqueous solution is replaced by another ionic species. Ion exchange in water treatment involves passing of water through an ion exchange polymer which is a water insoluble substance capable of exchanging some of its ions with ions of similar charge in the aqueous media. As (Equation 2 and 3) shows that HAp can remove fluoride through ion exchange and electrostatic interaction to form thermodynamically more stable fluorapatite ($Ca_{10}(PO_4)_3F_2$), or mixed fluoridated HAp ($Ca_{10}(PO_4)_3$(OH, F)) (Sundaram et al., 2008).

According to several natural organic materials possess ion exchange property or this property can be added to them through chemical modification (Kumar & Jain, 2013). This property has been applied in preparation of ion exchangers from natural materials such as wood, fibers, peat, and coal through modification using nitric acid as an oxidant or concentrated sulphuric acid to introduce the sulphonic acid group. The advantage of this method is high productivity (90-95 % fluoride removal) and retains the superiority of water. The limitation of this method is interference because of the presence of other anions like sulphate, carbonate, phosphate and alkalinity and it requires longer reaction period.

$$Ca_{10}(PO_4)_6(OH)_2 + 2F^- \rightarrow Ca_{10}(PO_4)_6F_2 + 2OH^- \quad \text{.....(2)}$$

$$Ca_{10}(PO_4)_6(OH)_2 + F^- \rightarrow Ca_{10}(PO_4)_6FOH + OH^- \quad \text{.....(3)}$$

2.5.3. Chemical Precipitation Method

This method involves the transformation of dissolved materials into insoluble solids followed by their removal through sedimentation or filtration. In this case fluoride is precipitated from the aqueous phase as insoluble calcium fluoride. In fluoridation process lime and alum are commonly used as precipitating agents. Nalgonda technique has been commonly used and it is based on addition of lime and alum in a two-step process. At the point when alum is added to water, basically two reactions happen. In the first reaction, alum reacts with an alkalinity's portion to deliver insoluble aluminum hydroxide ($Al(OH)_3$). In the second reaction, alum reacts with fluoride ions in the water. The advantage of this method is more practical when contrasted with other defluoridation technique and technique is easy to understand.

The disadvantage of this method is it produces large amount of sludge which poses disposal problems and requires large amount of chemicals which must be added daily. It also alters the pH of water hence adjustment of pH is needed (Ayoob et al., 2008).

2.5.4. Adsorption Method

Adsorption is the bond of molecules species from bulk solution for a surface of a solid by physical or chemical forces. Adsorption procedures include the water's entry through a contact bed where fluoride is removed by ion exchange or surface chemical reaction with the solid bed matrix. Adsorption technique is efficient and can remove ions over an extensive variety of pH to a lower left over concentration than precipitation (Ghorai & Pant, 2005).

A few adsorbent materials have been attempted in the past to check their possibilities and techno-economic feasibility as defluoridation specialists. Activated alumina, activated carbon, activated alumina coated silica gel, calcite, activated saw dust, activated coconut shell powder, groundnut shell, coffee husk, rice husk, tri-calcium phosphate, activated soil sorbent, spent tea and so on various adsorbent materials reported in literature. Hydroxyapatite has been shown to be effective adsorbents for water pollutants. HAp was studied as a fluoride sorbent either at fixed conditions or by considering the effect of some important parameters such as contact time, sorbent dose, particle size, solution pH, temperature, the presence of other anions and fluoride concentration (Jiménez-Reyes & Solache-Ríos, 2010). Adsorption using these materials may be due to formation of Van der Waals forces, ion exchange, hydrogen bonding, ligand exchange or chemical modification on the surface of adsorbent. Large specific surface area of HAp is very important for adsorption. The advantage of this method is high productivity for fluoride removal and can remove up to 90% fluoride, produce high quality water and regeneration is conceivable. This method has limitations in that it disposal of depleted adsorbents and concentrated regenerated makes issue and interference because of the vicinity of different anions may bring about competition for active sites on adsorbent.

2.6. Factors Affecting the Rate of Fluoride Removal

The factors that affecting the rate of fluoride removal are contact time, pH, adsorbent dose and initial fluoride concentration. Several researchers have studied the effect of contact time, pH, adsorbent dose and initial fluoride concentration (Akafu et al., 2019, Getachew et al., 2015 and Sundaram et al., 2008).

2.6.1. Effect of Contact Time

Contact time between the adsorbing material and the aqueous solution is a major factor in fluoride removal. A high number of active sites at the initial stage lead to high diffusion of fluoride towards the adsorbent surface and after saturation of the active sites, no further adsorption were carried out on the residual fluoride concentration. Studies have shown that the rate of removal of pollutants from water using nanomaterial is higher at the beginning of the remediation process. This is because as the interaction process progresses the sites for the reaction becomes exhausted resulting in lower uptake rate of the pollutant (Mbugua et al., 2014). Therefore, this parameter determines the rate of mass transfer from the solution to the surface of the adsorbent, and the data were used to study the kinetic study of batch adsorption. This trend was observed on defluoridation processes that reported by (Tang et al., 2018).

2.6.2. Effect of pH

The adsorption process is controlled by the pH of the adsorbate solution. The pH of the solution has a significant effect on the removal of fluoride ions from water since it determines the surface charge of the adsorbent. The removal of fluoride decreases with increasing pH of the solution (Getachew et al., 2015). At low pH values the removal of fluoride ions from water was high. The main reason behind the maximum defluoridation at low pH values may be because of the presence of a large number of H^+ ions at these pH values. Also, at high pH there is abundance of hydroxide ions which hinder the diffusion of fluoride ions. This leads to neutralization of the OH^- ions on the adsorbed surface and hence reduction of the hindrance to the diffusion of fluoride ions. As pH of the system controls the adsorption capacity through its influence on the surface properties of the adsorbent and species of adsorbate in solution, the effect of pH on adsorption of fluoride was studied in the pH range of 2.0 –10.0. Therefore, before defluoridation test the maximum removal efficiency of pH value must be determined. The best adsorption and fluoride uptake capacity both occurred at pH 6 (Bhaumik & Kumar, 2014).

2.6.3. Effect of dosage

The adsorbent dose on the fluoride in water can influence the removal capacity of fluoride ion. The fluoride removal efficiency is directly proportional to the adsorbent dose.

An increase in adsorbent dose, the rate of removal also increased because of availability of additional active sites (Getachew et al., 2015). This has been attributed to higher availability of surface and pore volume at higher doses.

2.6.4. Effect of Initial Concentration

The initial fluoride concentration has an influence on the removal capacity of the adsorbent. The capacity of the nanomaterial gets sharply exhausted with increase in the initial concentration of the fluoride in aqueous phase This is due to the fact that the adsorption sites for a fixed amount of nanomaterial are limited and become saturated at high concentration (Palanisamy et al., 2012).

2.7. Adsorption Isotherm

Adsorption isotherm is the relationship between the adsorbate in the liquid phase and the adsorbate adsorbed on the surface of the adsorbent at equilibrium at constant temperature. Adsorption isotherms are very important in order to design adsorption processes; they also provide adsorption capacity of the adsorbent under the studied conditions. Langmuir and Freundlich isotherms provide information on the nature and physic-chemical interactions involved in the adsorption. These two-parameter models are simple and give a good description of experimental behavior in a large range of operating conditions. The Langmuir adsorption isotherm is used to describe the equilibrium between adsorbate and adsorbent system, where the adsorbate adsorption is limited to monolayer at or before a relative pressure of unity is reached. Freundlich adsorption isotherm is considered to be a multilayer process in which the amount of adsorbed solute per unit adsorbent mass increases gradually. To determine whether the adsorption favors is the Langmuir or the Freundlich model, to compare the result of R^2 value.

2.8. Adsorption Kinetics Model

Adsorption kinetics model is very important to know the rate at which the adsorption process takes place and the factors that control the rate of the process. The adsorption kinetic models describe the rate of uptake of the adsorbate molecule; in this case, fluoride ion onto adsorbent, the rate depends on the physicochemical characteristics of the adsorbate and adsorbent, pH, temperature, and concentration. Pseudo first order and pseudo second order models are very common to describe adsorption kinetics model.

To determine whether the adsorption favors is the Pseudo-first-order kinetic model or pseudo-second-order kinetics model, to compare the result of R^2 value.

2.9. The pH at point of zero charges (pHpzc)

The point of zero charge is generally described as the pH at which the net charge of total particle surface (adsorbent's surface) is equal to zero. Determination of the pHpzc value helps to identify the working pH value for adsorption studies. The surface charge of adsorbent below pHpzc value would be positive so that the anions can be adsorbed on the surface of adsorbent. The surface charge of adsorbent above pHpzc value would be negative so that the cations can be adsorbed. At pH < pH pzc the surface charge is positive, favoring anion adsorption. At pH > pH pzc the surface charge is negative, favoring cation adsorption (Chinnakoti et al., 2017). The pH point of zero charges values for the synthesized HAp powder at an optimized operational parameters were reported by (Workeneh et al., 2019, Medellin-castillo et al., 2014).

3. MATERIALS AND METHODS

3.1. Study Sites Description

The synthesis and characterization of HAp & Fe-HAp with SEM, TGA/DTA and XRD were carried out in Adama Science and Technology University. The characterization of FTIR was carried out in Bahar Dar University. Evaluation of defluoridation of water was conducted in the Oromia Self-Help Organization Fluoride Removal Technology Center laboratory at Mojo town. The real water sample was taken from Oromia region, East Shewa Meki district, and Tuch Dambali site. The antibacterial activity was carried out at Adama public health research and referral laboratory.

3.2. Materials

3.2.1. Chemicals and Reagents

The chemicals that used for this research are (Ca $(NO_3)_2 \cdot 4H_2O$, 98 %, $(NH_4)_2HPO_4$, 97 %, CO $(NH_2)_2$, 99 %, HNO_3, 69 %, NaCl, 99.5 %, CH_3COOH, 99.7 %) all are LOBA CHEMIE PVT.LTD and India chemicals. Distilled and tap water (H_2O), Fe $(NO_3)_3.9H_2O$, TECHNO PHARM CHEM. India, 98 %, NaF, BDH Chemicals Ltd. England, 97 %), $Na_2C_6H_2O_7$, BDH Chemicals, England, 99 %, $C_{10}H_{16}N_2O_8$, Brulux Laboratories (P), Ltd, India,99 %, and NaOH, SIGMA-ALORICH, Sweden, 98 %. Calcium nitrate tetrahydrate, Di-ammonium hydrogen orthophosphate and Iron nitrate nonahydrate were used as precursor to synthesize the HAp and Fe-HAp. All aqueous solutions were prepared using distilled water.

3.2.2. Apparatus and Instruments

The following laboratory apparatus and Instruments were used for the experiments: Funnel, dropper, spatula, sample holder tube, mortar with pestle, beaker (50, 100, 250 and1000 mL), conical flask (250 mL), measuring cylinder (10 and 50 mL), volumetric flasks (50, 100, 500 and 1000 mL), magnetic stirrer with hot plate, filter paper, crucible, electronic balance (Adam Equipment, Model WL 3000, UK), mechanical shaker (model SK 300, Japan), pH meter (HANNA instrument, HI 96107, Italy), furnace (model BK-5-12GJ, Japan), oven (Digit heat, J. P. Selecta, Spain), and fluoride ion selective electrode (Orion Model 96-09, USA).

Thermo gravimetric analysis/ Differential thermal analysis (Model DTG-60H), Fourier-Transform Infrared (Model FT/IR-6600 type A, Japan), Scanning electron microscope (Model JEOL JCM-6000plus, Japan) and X-ray diffractometer (XRD-700, Shimadzu Co., Japan).

3.3. Methods

3.3.1. Synthesis of HAp

The preparation of hydroxyapatite was carried out using a modified procedure reported by (Volkmer et al., 2008). Accordingly, 50 mL of 0.6 M aqueous solutions of Ca $(NO_3)_2.4H_2O$ and 50 mL of 0.36 M aqueous solutions of DAP were added into 250 mL Pyrex beaker and continuously stirred with magnetic stirrer for 30 min till a white precipitate was formed by adjusting the molar ratio of Ca/P to 1.67. Concentrated HNO_3 was added to dissolve the white precipitate and to adjust the pH value to 1.5 with stirring for 5 min. The mole of urea (Table1) was added to the clear solution, and homogenized by stirring with a magnetic stirrer for 30 min at room temperature. The homogenized solution was heated on a hot plate at 100 ℃ for 2.5 hr to remove the excess water. The gel agglomerate synthesis product was dried in oven at 200 ℃ for 1 hr. Then, the dried gel agglomerate synthesized HAp powder was stored in sample holder and taken for further characterization. After TGA/DTA characterization the dried HAp was calcined at 700 ℃ for 2 hr.

Table 1: Batch compositions for synthesis HAp

Sample code	Amount Composition			
	$Ca(NO_3)_2.4H_2O$ Mole	$(NH_4)_2HPO_4$ Mole	Urea Mole	Combustible amount (urea to calcium precursor mass ratio)
HAp_1	0.03	0.018	0.118	1
HAp_2	0.03	0.018	0.236	2
HAp_4	0.03	0.018	0.472	4

Where HAp_1, HAp_2 and HAp_4 represent the urea to calcium precursor mass ratio 1:1, 2:1 and 4:1 in which the synthesized HAp, respectively. (Table1) shows that the Ca/P molar ratio was maintained at the value of 1.67 for all synthesized HAp_1, HAp_2 and HAp_4.

3.3.2. Synthesis of Fe-HAp

The preparation of Fe-HAp was carried out using a modified procedure reported by (Kaygili et al., 2014). Fe-HAp was synthesized by using different mole of Fe and keeping other precursor's mole constant. $(Ca_{10-x}\ Fe_x\ (PO_4)_6(OH)_2$ with x = 0.01, x = 0.03, x = 0.05, x = 0.07 and x = 0.1. The values of x were obtained by setting the atomic ratio of Fe/ [Fe + Ca] as 0.1 %, 0.3 %, 0.5%, 0.7 % and 1 %, respectively. Ca $(NO_3)_2.4H_2O$ and Fe $(NO_3)_3.9H_2O$ were dissolved together in distilled water in beaker to obtain 50 mL [Fe + Ca] containing solution. Then, $(NH_4)_2HPO_4$ was dissolved in distilled water in another beaker to obtain 50 mL P-containing solution.

50 mL of 0.6 M aqueous solutions of Ca $(NO_3)_2.4H_2O$ and Fe $(NO_3)_3.9H_2O$ [Ca + Fe] and 50 mL of 0.36 M aqueous solutions of DAP were added into 250 ml Pyrex beaker and continuously stirred with magnetic stirrer for 30 min till a precipitate was formed. Concentrated HNO_3 was added with stirring for 5 min to dissolve a precipitate and to adjust the pH value at 1.5. The mole of urea (Table2) was added as fuel to the clear solution which was homogenized by stirring with a magnetic stirrer for 30 min at room temperature. The homogenized solution was heated on a hot plate at 100 ℃ for 2.5 hr to remove the excess water. The gel agglomerate synthesis product was dried in oven at 200 ℃ for 1 hr. Then, the dried gel agglomerate synthesized HAp powder was stored in sample holder and taken for further characterization. After TGA/DTA characterization the dried Fe-HAp was calcined at 700 ℃ for 2 hr.

Table 2: Batch composition for synthesized Fe-HAp

Sample Code	Amount Composition			
	$Ca(NO_3)_2.4H_2O$ Mole	$Fe(NO_3)_3.9H_2O$ Mole	$(NH_4)_2HPO_4$ Mole	Urea Mole
$Fe_{0.01}$ HAp	0.02997	0.00003	0.018	0.472
$Fe_{0.03}$ HAp	0.02991	0.00009	0.018	0.472
$Fe_{0.05}$ HAp	0.02985	0.00015	0.018	0.472
$Fe_{0.07}$ HAp	0.02979	0.00021	0.018	0.0472
$Fe_{0.1}$ HAp	0.0297	0.0003	0.018	0.0472

The mass of urea was fixed to HAp_4 from the preliminary test conducted on the fluoride removal efficiency of HAp_1, HAp_2, and HAp_4 from aqueous solution under the same condition. Hence, HAp_4 has high removal efficiency of fluoride and therefore Fe was doped into HAp_4. (Table 2) shows that the moles of DAP and urea were constant but, the moles of calcium and iron precursors were changed. But, the (Fe+Ca)/P molar ratio was maintained at the value of 1.67 for all optimized Fe-HAp.

3.4. Characterization Techniques

3.4.1. Thermogravimetric Analysis and Differential thermal analysis (TGA/DTA)

TGA/DTA analysis was used (Model DTG-60H) for the determination of the calcination temperature, weight loss, energy gain or loss. 10 mg of Hap_4 and 12.083 mg $Fe_{0.05}$HAp were taken and placed in the alumina crucible for TGA/DTA analyzed at the heating rate of 20 ℃/ min with a constant supply of non-stop glide of nitrogen. The TGA/DTA of Hap_4 and $Fe_{0.05}$HAp were measured in the temperature range 31.26 ℃ to 800 ℃ and 23.79 ℃ to 1001.71 ℃, respectively.

3.4.2. Fourier-Transform Infrared Spectroscopy (FTIR)

FTIR analysis was used to determine the presence of different functional groups and organic impurities. FTIR (Model FT/IR-6600 type A) was used in a transmission mode of the mid-infrared range with wave numbers from 400 to 4000 cm^{-1} using the KBr pellet technique. KBr pellet technique is widely used for FTIR spectroscopy with accuracy reading, because the KBr does not show any absorption spectrum in IR region and it has a 100 % transmission gap in the range of wave number (400 - 4000 cm^{-1}). 2 mg of synthesized material (HAp_4 and $Fe_{0.05}HAp$) powder compressed with 200 mg of KBr to form 12 mm diameter pellet and then placed on a specimen holder. Spectra were measured between in the range of 4000 cm^{-1} to 400 cm^{-1} at a resolution of 4 cm^{-1}, with number of scans 8 and scanning speed 2 mm/sec.

3.4.3. Scanning electron microscopy (SEM)

The synthesized HAp_4 and $Fe_{0.05}HAp$ morphology was analyzed using SEM (model JEOL JCM-6000plus, Japan). Electron beam energy of HAp_4 and $Fe_{0.05}HAp$ were carried out at accelerate voltage at 15 kV and magnification of 600. The synthesized HAp_4 and $Fe_{0.05}HAp$ powder were mounted on a sample holder followed by coating with a smart coater (Gold) and then, the sample was scanned using SEM.

3.4.4. X–ray diffraction (XRD)

The crystallite size, crystallite structure, miller indices and space group present in a synthesized HAp_4 and $Fe_{0.05}HAp$ were characterized using an X-ray diffractometer (XRD-700, Shimadzu Co., Japan). A Cu target for generating a Cu Kα radiation (λ = 0.154056 nm) was used as the incident X-ray beam at an accelerating voltage of 40 kV and a current of 30 mA. The powder samples were mounted on a flat XRD plate and scanned in the range 10º to 85º at room temperature in the continuous scan speed 3°/min. The crystal structure, phase purity of HAp_4 and $Fe_{0.05}HAp$ powder were studied from the XRD pattern obtained in the step scanning mode in the same 2θ range. The step size and the time per step were 0.02° and 0.40 sec respectively.

3.5. Collection of Water Sample for the Defluoridation Test

The real water sample was collected from Tuch Danbali located at East Shewa Meki district. The sample was taken in 500 mL in sample holder. Before the sample was taken in sample holder, a sample holder was washed three times by distilled water because to avoid contamination.

Then, the pH and fluoride ion concentration of ground water were measured. The pH of the collected real water was 8.2 and its fluoride concentration was 6.9 mg/L. Then, 20 mL of ground water, 15 mL of distilled water and 3 mL of TISAB were added into one beaker. Then, the concentration of fluoride in ground water was measured by using fluoride ion selective electrode.

3.6. Determination of fluoride

3.6.1. Preparation of Stock Solution

2.21 g of sodium fluoride was weighed and transferred into 1000 mL volumetric flask. Then, it was dissolved by distilled water and diluted to 1 L. The prepared solution containing 2210 mg/L stock solution of sodium fluoride or 1000 mg/L stock solution of fluoride ion. From the stock solution 100 mg/L intermediate solution was prepared. From this intermediate solution, four samples of fluoride solutions of 10, 15, 20 and 25 mg/L were prepared by serial dilution which was used for optimization of parameters.

3.6.2. Preparation of Total Ionic Strength Adjustment Buffer (TISAB)

A TISAB is employed to regulate samples and standards to the same ionic strength and pH. TISAB is essential in fluoride ion selective electrode measurements because it masks minor changes made in the ionic strength of the solution, maintain pH constant and hence increases the accuracy of the reading. 7 g of tri-sodium citrate ($Na_2C_6H_2O_7$), 58 g sodium chloride (NaCl), and 2 g EDTA were dissolved into 500 mL of distilled water. Then, 57 mL of glacial acetic acid was added into the solution. Finally, 5 M of sodium hydroxide was added till the pH of the solution was reached at 5.3 and then the solution was transferred to a 1000 mL volumetric flask, and filled up to the mark using distilled water (Akafu et al., 2019).

3.6.3. Calibration of the Electrode

Before calibration of the electrode, the reference electrode hole was filled with KCl solution and the electrode was stored in TISAB solution. Then, the electrode was rinsed with distilled water to minimize contamination. 2 ppm, 4 ppm, 6 ppm, 8 ppm and 10 ppm of fluoride solution were prepared. To 30 mL of each five fluoride solutions 3 mL of TISAB was added in order to maintain pH constant and increases the accuracy of the reading. Then, the potential response of fluoride ion was measured starting from low concentration to high concentration using FISE.

Finally, to determine the slope of the graph, the potential response (E in mV) versus the negative logarithm of concentration (- log C in mg/L) was plotted.

3.7. The pH at point of zero charges

To identify the working pH value for adsorption studies the point of zero charge was determined before optimization of pH. 50 mL of 0.1 M NaCl solutions were taken in eight conical flasks with pH range 2 – 9 by 1 pH increment and the pH was adjusted by using 0.1 M HCl and 0.1 M NaOH. Then, 0.5 g of $Fe_{0.05}$HAp powder was added to each solution and vibrated by using mechanical shaker at a speed of 150 rpm for 10 hr. Then, the adsorbent was separated from the solutions by using filter paper and funnel. After equilibration the final pH of each sample was measured by using pH meter. Then, the change in pH (ΔpH) was calculated (ΔpH = final pH – initial pH). Finally, to determine the pH at pzc, the graph of change in pH vs. final pH was plotted.

3.8. Batch adsorption studies

Adsorption studies consist of adsorption kinetics and adsorption isotherm model. Adsorption kinetics is used to understand sorption rate and the effect of contact time on adsorption. Adsorption isotherm model used to understand sorption mechanism and effect of concentration on adsorption. In this study, the effect of major parameters like pH, adsorbent dose, contact time and initial fluoride concentration were optimized to investigate the maximum defluoridation efficiency of the synthesized $Fe_{0.05}$HAp.

3.8.1. Effect of pH

To study the effect of pH on defluoridation, 50 mL of 10 mg/L of fluoride solution was taken and pH values was adjusted to 3, 5, 7 and 9 by using 0.1 N HCl and 0.1 N NaOH and the adsorbent dose was remained constant acidic, neutral, and basic media.

That is 0.5 g of synthesized $Fe_{0.05}$HAp was added to each of the solution and tested separately and stirred for 1 min to reach equilibrium. Then, the solution was shaken by using mechanical shaker at a speed of 150 rpm for 5 hr. After a given time was completed the solution was filtered. 3 mL of TISAB was added to each solution in order to maintain pH constant and stirred with magnetic stirrer. Then, the F^- ion concentration of filtrate solution was determined by using fluoride ion selective electrode. Finally, the pH versus percentage removal graph was plotted to explain the effect of pH on adsorption performance of the $Fe_{0.05}$HAp adsorbent.

3.8.2. Effect of Adsorbent Dosage

To study the effect of the synthesized $Fe_{0.05}$ HAp dose on defluoridation, 50 mL of 10 mg/L of fluoride solution was adjusted to a pH of 3, which have high removal efficiency. Then various dosages of $Fe_{0.05}$HAp (0.1 g, 0.3 g, 0.5 g, 0.7 g, and 0.9 g) were added into the solution. Then, the solution was shaken by mechanical shaker at a speed of 150 rpm for 5 hr. After 5 hr was completed the solution was filtered. 3 mL of TISAB was added to each solution in order to maintain pH constant and stirred with magnetic stirrer. Then, the F^- ion concentration of filtrate solution was determined by using ion selective electrode. Finally, adsorbent dosage versus percentage removal graph was plotted to explain effect of adsorbent dose on the adsorption performance of the $Fe_{0.05}$HAp adsorbent.

3.8.3. Effect of Contact Time

To study the effect of contact time on defluoridation, 50 mL of 10 mg/L of fluoride solution was taken and then, the pH was adjusted at 3 which have high removal efficiency. Then 0.7 g of $Fe_{0.05}$HAp with high removal efficiency of fluoride was added into each solution. Then, the solution was shaken by mechanical shaker at a speed of 150 rpm for different contact time (1 hr, 3 hr, 5 hr and 7 hr). After these periods of intervals, the solution was filtered. 3 mL of TISAB was added to each solution in order to maintain pH constant and stirred with magnetic stirrer. Then, the F^- ion concentration of filtrate solution was determined by using ion selective electrode. Finally, time versus percentage removal graph was plotted to explain the effect of contact time on adsorption performance of the $Fe_{0.05}$HAp adsorbent.

3.8.4. Effect of initial concentration of fluoride ion

To study the effect of initial concentration of fluoride ions on defluoridation, 50 mL of fluoride solutions with different concentration (10 mg/L, 15 mg/L, 20 mg/L and 25 mg/L) were taken and then, the pH was adjusted at 3 which have high removal efficiency of fluoride. Then 0.7 g of $Fe_{0.05}$HAp with high removal efficiency of fluoride was added into each solution. Then, the solution was shaken by mechanical shaker at a speed of 150 rpm for 3 hr which have high removal efficiency of fluoride. After 3 hr was completed the solution was filtered. 3 mL of TISAB was added to each solution in order to maintain pH constant and stirred with magnetic stirrer. Then, the F^- ion concentration of filtrate solution was determined by using FISE.

Finally, initial concentration versus percentage removal graph was plotted to explain the effect of initial concentration of fluoride adsorption performance of the $Fe_{0.05}$HAp adsorbent.

3.8.5. Defluoridation Test of real water

The concentration of fluoride ion in ground water was measured by using optimized parameters. 50 mL of 6.9 mg/L of ground water was taken into a beaker. 0.7 g $Fe_{0.05}$HAp dosage was added into the solution in the beaker. Then, the solution was shaken by mechanical shaker at a speed of 150 rpm for 3 hr at pH 3. After 3 hr was completed the solution was filtered. Then, 3 mL of TISAB was added to the solution in order to maintain pH constant and stirred with magnetic stirrer. Finally, the F^- ion concentration of filtrate solution was determined by using ion selective electrode.

3.8.6. Desorption and Regeneration of Adsorbent

To study the desorption and regeneration of adsorbent on defluoridation, 50 mL of 10 mg/L of fluoride solution was taken in beaker and the pH of the solution was adjusted at 3. Then 0.7 g of $Fe_{0.05}$HAp powder was added and shaken by using mechanical shaker at a speed of 150 rpm for 3 hr. After adsorption the adsorbent was separated by filtration. The filtrate concentration of fluoride was measured and removal efficiency of fluoride was calculated for the first cycle. Then, the residual of adsorbent was dispersed in 50 mL of 1 N NaOH to be desorbed and shaken for 1 hr. After 1 hr the solution was decanted and the residual adsorbent was dried in oven for 30 min at 150 ℃. The dried residual adsorbent mass was measured and regenerated for fluoride adsorption again. Five cycles of desorption and regeneration was performed using the same procedure.

3.9. Antibacterial Activity

Antibacterial activities were carried out against two bacterial strains; gram-negative *E. coli* ATCC 25922 and gram positive *S. aureus* ATCC 25923 bacteria at Adama public health research and referral laboratory by disc diffusion method. Bacterial cultures were maintained on Blood agar at 37 ℃. Bacterial strains were taken from ATCC and grown aerobically on Blood Agar for 24 h at 37 ℃ and 0% CO_2. Bacterial suspension was prepared by taking it from blood agar and dissolving in sterile normal saline until the concentration of bacterial suspensions were achieved to1× 108 colony CFU/mL by comparison with the 0.5 McFarland Standard.

100 μL of 24 hr standardized culture of test bacteria was first evenly spread onto the surface of the Muller-Hinton agar plates using sterile cotton swabs. A sterile swab is used to inoculate the surface of the media in Petri dishes with making three rotations with an angle of 60° to ensure a homogeneous growth. The plates were then turned upside down. 6 mm diameter of filter paper was prepared and placed in different areas of the disc. The antibiotic Contrimoxazole was used as the positive control, and DMSO solvent was used as the negative control. 30 mg of each prepared samples were dissolved in 1 mL dimethyl sulfoxide (DMSO) and formed 30 mg/mL. From 30 mg/mL concentration of sample, 15 mg/mL, 7.5 mg/mL and 3.75 mg/mL were prepared by diluting serially for pure HAp and $Fe_{0.05}$HAp. Then, 6 mm diameter disc was saturated with 20 μL from each concentration and 20 μL of 0.5 mg/ mL of Contrimoxazole and placed on a plate and covered with lids and incubated at 37 °C at 37 °C and 0% CO_2 for 24 hr. Antibacterial activity was evaluated by measuring the diameter of the inhibition zone observed around the discs. The inhibition zone reveals the bacteria sensibility to toxic agents so that the disinfectant-sensitive strains show large inhibition diameter and the resistant strains show a smaller or zero inhibition diameter. This diameter can be compared to the critical diameters of antibiotics Contrimoxazole and digital images were captured (Dadi et al., 2019).

4. RESULTS AND DISCUSSION

In this section, the characterization of synthesized HAp_4 and $Fe_{0.05}HAp$, the application of synthesized HAp_4 and $Fe_{0.05}HAp$ for the removal of fluoride ion from ground water and investigation of antibacterial activities, adsorption study and the result of optimization parameters are discussed.

4.1. The pH at point of zero charge

The pHpzc determination of $Fe_{0.05}HAp$ was carried out at pH 2 - 9 by one pH unit increment (Table 3). Determination of the pHpzc value helps to identify the working pH value for adsorption studies. Figure 2 shows the point of zero charge is 7.5 in agreement with (Mourabet et al., 2012, Mehta et al., 2016) . Below the pzc the adsorbent has positive charge while above the point of zero charge it has negative charge. The higher fluoride adsorption was occurred under pH 7.5 due to highly electrostatic attraction between the positively charged adsorbent surface and highly electro negative fluoride ions. The low removal efficiency of fluoride was achieved above pH 7.5; this is due to weak electrostatic attraction between the negatively charged adsorbent surface and highly electro negative fluoride ions.

Table 3: The different pH value used for termination of pzc

Initial pH	2	3	4	5	6	7	8	9
Final pH	3.56	4.64	5.51	6.46	6.85	7.29	7.69	7.78
Change in pH	1.56	1.64	1.51	1.46	0.85	0.29	- 0.31	-1.22

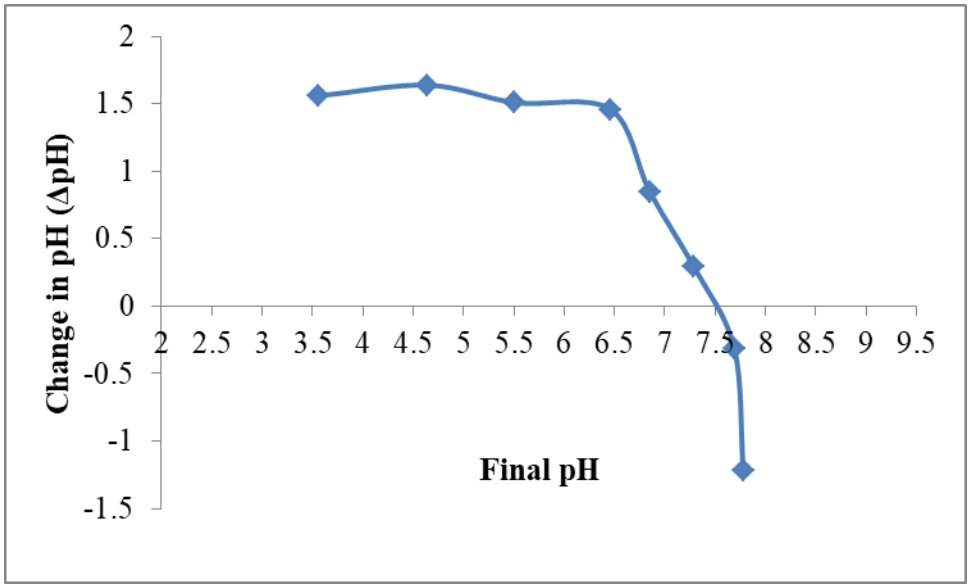

Figure 1: Plot of Δ pH vs. final pH of the adsorbent to determine the point of zero charge of the adsorbent surface performed at 0.5 g $Fe_{0.05}$ HAp, 50 mL of 0.1 M NaCl solution and contact time of 10 hr.

4.2. Calibration of Fluoride Ion Selective Electrode

The fluoride ion selective electrode was calibrated by using different fluoride ion concentration of standard solution. The graph of calibration curve was plotted by potential response (E in mV) vs. negative logarithm of fluoride concentration (- LogCe in mg/L) as shown in (Figure 3). The slope of the graph and R^2 were determined from the curve to check the accuracy of the measurement. The slope of fluoride ion should be in the range 54 - 60 mV L mg^{-1}. From (Figure 3) the slope was observed between the standard intervals with good R^2 values. From the plotted graph, the slope was found to be 57.93 mV L/mg and R^2 value 0.9954, which is nearest to one. Therefore, the fluoride concentrations were calculated using the regression equation E = 57.93 (- Log Ce) - 64.876 (Table 4 and Figure 2).

Table 4: Potential response recorded and negative logarithm of fluoride concentration

Potential response (E) in mV	Negative logarithm of fluoride concentration (- LogC in mg/L)
- 83	- 0.301
- 98	- 0.602
- 111	- 0.778
- 117	- 0.903
- 123	- 1

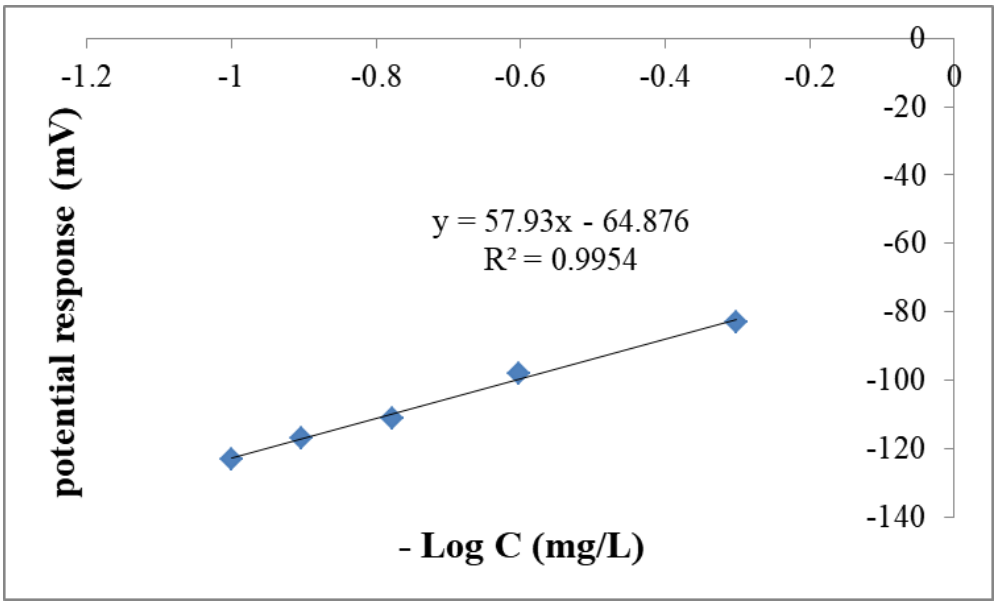

Figure 2: Electrode calibration E versus – LogC of fluoride concentration

4.3. Adsorption Studies

4.3.1. Optimization of Different Parameters for Adsorption Study

The effect of different parameters were optimize such as; pH, dosage of adsorbent, contact time and initial concentration of fluoride ion. Before parameters optimization, the effectiveness of optimized pure HAp and Fe-HAp were evaluated. The fluoride removal efficiency of HAp for HAp_1, HAp_2 and HAp_4 were measured as 90.7 %, 92.1 % and 95.1 %, respectively. After the removal efficiency of HAp_1, HAp_2 and HAp_4 were evaluated; Iron was doped with different mole ratios into HAp with high fluoride removal efficiency (HAp_4). Investigation on the fluoride removal efficiency of Fe-HAp again conducted for all Fe-HAp adsorbents. The removal efficiency of $Fe_{0.01}$HAp, $Fe_{0.03}$HAp and $Fe_{0.05}$HAp, $Fe_{0.07}$HAp and $Fe_{0.1}$HAp were measured to be 91.1 %, 91.8 %, 96.1 %, 93.2 % and 90.3%, respectively. As (Figure 3a) shows that as urea to calcium precursor mass ratio increases the removal efficiency of fluoride ion increases. As (Figure 3b) shows that as concentration of Fe-HAp increases the removal efficiency of fluoride ion increases up to $Fe_{0.05}$HAp. But after 0.05 mole of Fe-HAp the removal efficiency of fluoride ion decreases.

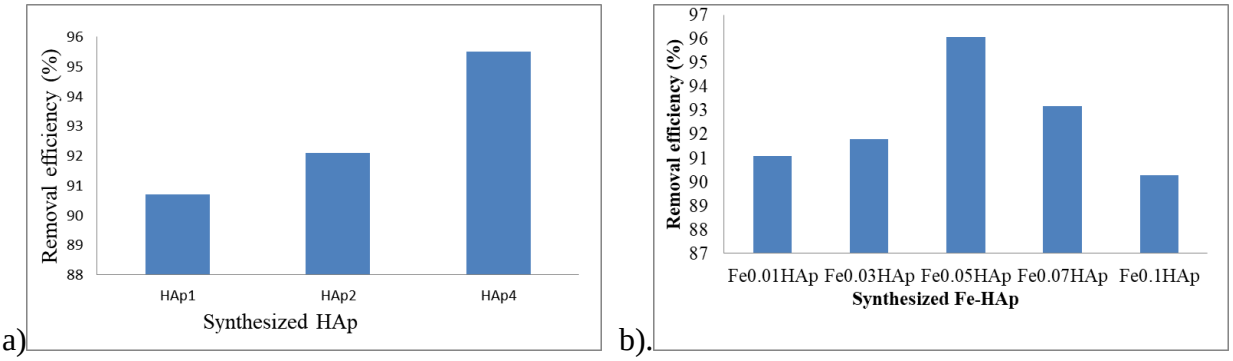

Figure 3: The effectiveness of HAp_4 and $Fe_{0.05}$HAp on the fluoride ion removal from aqueous solution using adsorbent dosage 0.5 g, pH 3, initial concentration of fluoride ion solution 10 mg/L, volume of fluoride solution 40 mL, and shaking speed 150 rpm for 5 hr.Removal efficiency of a) HAp and b) Fe-HAp by different ratio.

4.3.1.1. Effect of pH on removal of fluoride ion by $Fe_{0.05}$HAp

During the adsorption process, determination of pH of the solution was very important. The pH of the solution was tested in acidic, neutral, and basic media. At very low pH the acidity of solution was increased and adsorbent was dissolved.

Figure 4 shows that the maximum removal efficiency of fluoride ion was achieved at pH 3 which is 95.6 %. From the result of pH optimization, it was observed that at high pH values the removal of fluoride ion was low and high at low pH values. In acidic medium, where the concentration of H^+ ion is high and therefore $Fe_{0.05}$HAp surface gets positive charge which in turn attracts more fluoride ions and hence there is a significant increase in fluoride removal capacity at lower pH. The high uptake at low pH was attributed to the high concentration of hydrogen ions at low pH which increases the positive charge on the surface of the adsorbent leading to greater removal of fluoride ion (Chowdhury et al., 2011). At pH above the pzc, adsorption of fluoride ion was low because the $Fe_{0.05}$HAp surface was negatively charged, due to deprotonating of $Fe_{0.05}$HAp hydroxyl groups (Mourabet et al., 2012). There was repulsive force between the negatively charged of fluoride ion and the negatively charged adsorbent surface. Due to this repulsive force between the two negatively charged ions the removal of fluoride ion was decrease.

Table 5: Effect of pH on removal efficiency of fluoride ion

pH value	Remaining concentration of fluoride ion (mg/L)	Removal efficiency of fluoride ion (%)
3	0.44	95.6
5	0.60	94
7	0.89	91.1
9	1.38	86.2

(Table 5) shows that the remaining concentration of fluoride ion for each pH value. These remaining fluoride concentrations can be recorded from potential response. The removal efficiency of fluoride ion was calculated from remaining concentration of fluoride ion. The removal efficiency of fluoride ion at each pH clearly shows in Figure 4.

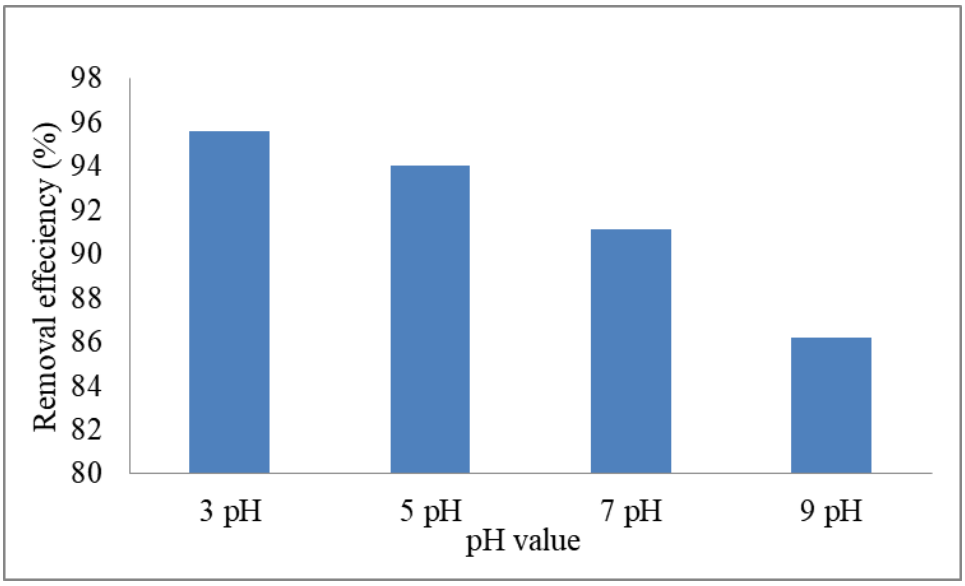

Figure 4: The effect of pH on the removal of fluoride ion was carried out by keeping all parameters constant like adsorbent dosage 0.5 g of $Fe_{0.05}$HAp, initial concentration of fluoride ion solution 10 mg/L, volume of fluoride solution 50 mL, and shaking speed 150 rpm for 5 hr. Effect of solution pH on removal efficiency of fluoride ion

4.3.1.2. Determination of adsorbent dosage

Determination of adsorbent dosage of the synthesized material was very important during the adsorption process. The effect of adsorbent dosage ($Fe_{0.05}$HAp) was optimized by taking different masses and by keeping all parameters constant. As (Figure 5) shows that the maximum removal efficiency of fluoride ion was achieved at adsorbent dosage of 0.7 g which is 96.1 %. As (Figure 5) result indicates that the removal efficiency of fluoride ion increases as $Fe_{0.05}$HAp dosage increases up to 0.7 g at optimum dose. This is because at high doses there is high availability of active sites. The number of binding sites resulting from increased adsorbent dosage and availability of more effective sites for interaction contributed to the observed result (Chowdhury et al., 2011). But the removal efficiency of fluoride was decreased at 0.9 g dosage due to the overlap or blocking of functional surface sites of adsorbent. Another reason is due to the depletion of fluoride in the solution with an increasing dose of the adsorbent.

Table 6: Effect of adsorbent dosage on removal efficiency of fluoride ion

Adsorbent dosage in g	remaining concentration fluoride ion in mg/L	Removal efficiency of fluoride ion in %
0.1	0.76	91.1
0.3	0.53	94.7
0.5	0.44	95.6
0.7	0.39	96.1
0.9	0.58	94.2

(Table 6) shows that the remaining concentration of fluoride ion in the solution for all five dose. The removal efficiency of fluoride ion for each adsorbent dose clearly shows in (Figure 5).

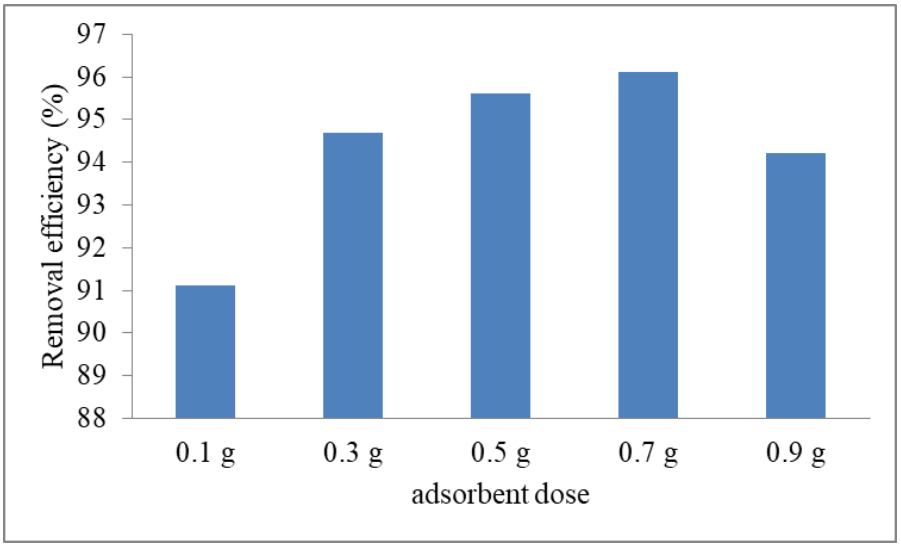

Figure 5: The effect of adsorbent dosage on the removal of fluoride ion was carried out by varying dose and by keeping all parameters constant like initial concentration of fluoride ion solution 10 mg/L, volume of fluoride solution 50 mL, pH 3, at shaking speed 150 rpm for 5 hr.

4.3.1.3. Determination of contact time

During adsorption process, determination of the effect of contact time is very important. The effect of contact time was optimized by varying the contact time and by keeping all parameters constant. (Figure 6) shows that a rapid fluoride removal was observed at the initial stage contact time until reaching equilibrium time with high removal efficiency. (Figure 6) shows that the maximum removal efficiency of fluoride ion was achieved at contact time 3 hr which is 98 %. As contact time increases from 1 hr to 3 hr the removal efficiency of fluoride ion was increased. This is due to a high number of active sites at the initial stage lead to high diffusion of fluoride ion towards the adsorbent surface. But after the equilibrium time is reached the removal efficiency of fluoride was decreased. This is due to the saturation of the active sites and no enough additional active sites of adsorbent with increasing contact time.

Table 7: Effect of contact time on removal efficiency of fluoride ion

Contact time in hr.	Remaining concentration of fluoride ion in mg/L	Removal efficiency of fluoride ion in %
1	0.73	92.7
3	0.2	98
5	0.39	96.1
7	0.86	91.4

(Table 7) show that the remaining concentration of fluoride ion at each contact time. All concentrations were calculated from potential response reading. The removal efficiency of fluoride ion at each contact time clearly shows in (Figure 6).

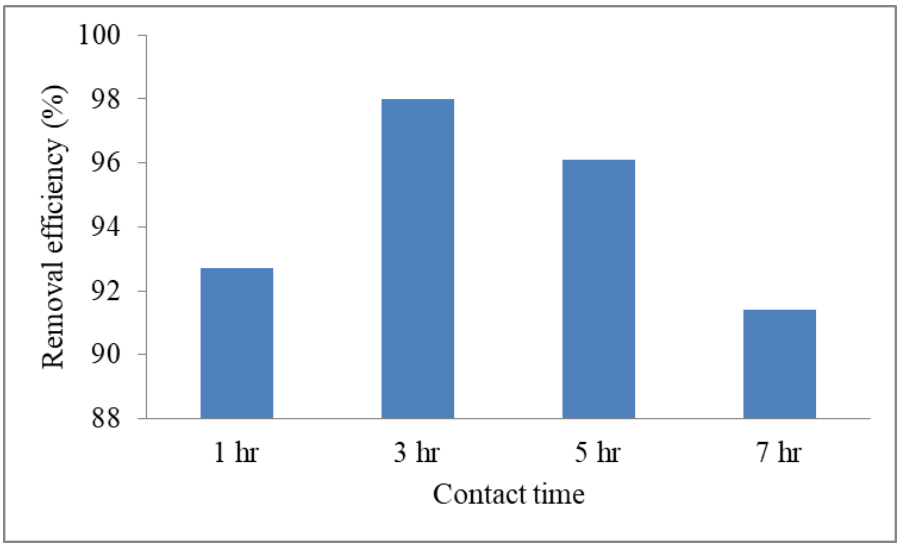

Figure 6: The effect of contact time was optimized by varying contact time and by keeping all parameters constant like initial concentration of fluoride ion solution 10 mg/L, volume of fluoride solution 50 mL, pH 3, adsorbent dose 0.7 g, at shaking speed 150 rpm.

4.3.1.4. Determination of initial concentration

The effect of initial concentration was determined by using varying initial concentration of fluoride and by keeping all parameters constant. (Figure 7) shows that the maximum removal efficiency of fluoride ion was achieved at initial concentration of 10 mg/L which is 98 %. There is high removal efficiency of fluoride at lower initial fluoride concentrations. This is because there is high active site of adsorbent surface at low concentration. From this study, the result indicates that, as the initial concentration of fluoride increases the removal efficiency of fluoride decreases. This is due to lack of sufficient surface area to accommodate more fluoride ions available in the solution. When the initial fluoride concentration increases for fixed mass of adsorbent there is no further removal of fluoride because all active site of adsorbent was occupied by fluoride at initial concentration.

Table 8: Effect of initial concentration on removal of fluoride ion

initial concentration in mg/L	Final concentration of fluoride ion in mg/L	Removal efficiency of fluoride ion in %
10	0.2	98
15	0.6	96
20	1.09	94.55
25	1.82	92.72

(Table 8) show that the final concentration of fluoride ion from each initial concentration. All final concentrations of fluoride ion were calculated from potential response reading. The removal efficiency of fluoride ion for all initial concentration clearly shows in (Figure 7).

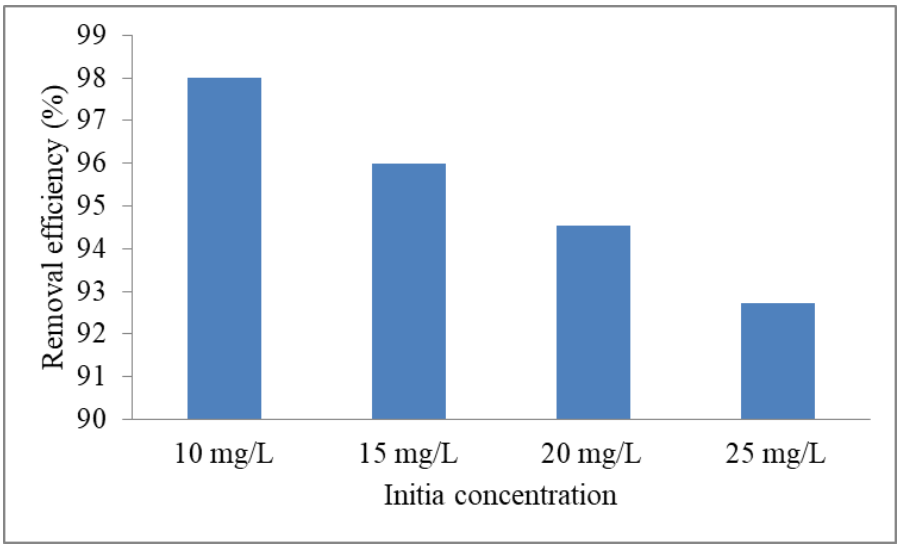

Figure 7: The effect of initial concentration on removal of fluoride ion was optimized by varying initial concentration and keeping all parameters constant like volume of fluoride solution 50 mL, optimized adsorbent dosage 0.7 g, pH 3, contact time 3 hr, at shaking speed 150 rpm.

4.4. Defluoridation of Ground Water

The fluoride removal performance of $Fe_{0.05}$HAp was evaluated by applying on groundwater. The fluoride removal performance of HAp_4 was not evaluated on ground water. This is because the removal efficiency of $Fe_{0.05}$HAp on synthetic water is greater than HAp_4. The removal efficiency and adsorption capacity of fluoride from ground water by $Fe_{0.05}$HAp powder were 82.9 % and 0.41 mg/g, respectively. After adsorption, the pH was decreased from 3 to 6.9, this is due to the negative fluoride ions neutralized some positive charges on the adsorbent surface. The result of fluoride removal efficiency indicated that $Fe_{0.05}$HAp from the groundwater samples was lower than that of the synthetic replicated NaF solutions. The Tuch Dambali groundwater samples were taken from the Ethiopian Rift Valley contained high concentration of co-ions. The pH of the real Tuch Dambali groundwater samples was measured to be 8.2. This pH shows basic water solution. In basic solution, the presence of high concentration of HCO_3^- and SO_4^{2-} ions interfere the uptake of fluoride ions by the adsorbents (Habuda-Stanić et al., 2014). The bicarbonate is great competitive adsorption with fluoride ions at the active site, on the surface of the sorbents. . The fluoride adsorption amount decreased rapidly from 78.1 to 52% with the increase of bicarbonate concentration 0 - 500 mg. The fluoride removal efficiency of synthetic water and groundwater study around Meki town were 98.8 % and 82.85 %, respectively, reported by (Workeneh et al., 2019). The fluoride removal of synthetic water and groundwater not equal, because the fluoride removal of groundwater was affected by co-ions as researcher describe.

4.5. Desorption and Regeneration of Adsorbent

Regeneration is used to reuse the adsorbent after desorption process was occurred. Regeneration techniques are very important to evaluate the application of adsorbent, its duration time, reduce the cost of the process and decrease the amount of undesired wastes. The adsorption of fluoride can be attributed to electrostatic interactions between the surface charge of adsorbent and fluoride ions in the aqueous solution (Medellin-castillo et al., 2014). The mechanism of adsorption (Equation 4 and 5), the interaction between the surface of adsorbent and the F^- do not lead to a chemical reaction because it has been demonstrated that the adsorption of F^- on adsorbent was reversible.

Desorption is the reverse process, that is release of the adsorbed adsorbate from the surface of adsorbent. Fluoride ion adsorbed on surface of hydroxyapatite was desorbed and released into solution by NaOH solution. In the determination of regeneration and desorption, the residual of adsorbent was washed and dispersed by using 1 N NaOH solution having pH of 13. This is because, with increasing pH, the fluoride ion captured in the hydroxyapatite structure was released into solution, exchanged by the hydroxide ion, an ionic substitution mechanism already described in other studies (Medellin-castillo et al., 2014; Sundaram et al., 2008).

The use of NaOH solutions was better used for regeneration and desorption of HAp when compared to other compounds. The OH^- remove the proton from adsorbent surface site and form water, the Na^+ remove F^- from adsorbent surface site and form NaF. The hydroxyapatite phase, the following reactions take place at elevated pH maintained during regeneration and desorption (Sarkar et al., 2015) .

$Ca_{(10-x)/2}Fe_{x/2}(PO_4)_3(OH) + F^-(aq) \rightarrow Ca_{(10-x)/2}Fe_{x/2}(PO_4)_3(OH) \equiv F^-$ ……..….. (4)

$Ca_{(10-x)/2}Fe_{x/2}(PO_4)_3 OH_2^+ + F^-(aq) \rightarrow Ca_{(10-x)/2}Fe_{x/2}(PO_4)_3 OH_2^+ F^-$ ……... (5)

$Ca_{(10-x)/2}Fe_{x/2}(PO_4)_3 OH_2^+ F^- + OH^-(aq) \rightarrow Ca_{(10-x)/2}Fe_{x/2}(PO_4)_3(OH) \equiv F^- + H_2O$ ……... (6)

$Ca_{(10-x)/2}Fe_{x/2}(PO_4)_3(OH) \equiv F^- + Na^+(aq) \rightarrow Ca_{(10-x)/2}Fe_{x/2}(PO_4)_3(OH) + NaF$……..... (7)

Adsorption in (Equation 4) take place at higher pH, in abundance of OH^- ions, while adsorption in (Equation 5) take place at lower pH , in abundance of H^+ ions. (Equation 6 and 7) shows the mechanism of fluoride removal from surface site of adsorbent. The % removal efficiency, adsorption capacity and % desorption efficiency fluoride by NaOH solution were calculated using the following (Equation 8, 9 and 10).

$$\% \text{ Removal efficiency} = \frac{C_o - C_f}{C_o} \times 100 \quad \text{……..… (8)}$$

$$\text{Adsorption capacity} = \frac{(C_o - C_f)}{m} \times V \quad \text{……... (9)}$$

$$\% \text{ Desorption} = \frac{C_{des.}}{C_{ads.}} \times 100 \quad \text{……..... (10)}$$

Where Co initial concentration (mg/L), Cf final concentration (mg/L), Cdes concentration of fluoride desorbed (mg/L) and Cads concentration of fluoride adsorbed (mg/L).

Table 9: The removal efficiency of regeneration and desorption

Initial concentration (mg/L)	Adsorption concentration (mg/L)	Desorption concentration (mg/L)	Removal efficiency of adsorption for regeneration (%)	Desorption efficiency (%)
10	9.8	9.43	98	96.22
10	9.11	8.72	91.1	95.72
10	8.72	8.32	97.2	95.41
10	8.25	7.85	82.5	95.2
10	8.02	7.6	80.2	94.76

From (Table 9) the regeneration removal efficiency of fluoride, the fluoride removal was decreased. This is because the mass of residual adsorbent was decreased, while the volume of solution and concentration of fluoride in solution were constant in all five cycles. Another reason is the fluoride adsorbed on adsorbent was not total desorbed. For every cycle, desorption of fluoride from residual adsorbent and regeneration of the residual adsorbent were measured (Table 9). After every cycle, regeneration and desorption the mass of the residual adsorbent was measured. The fluoride removal was changed by small amount. Therefore, the synthesized adsorbent was suitable for regeneration and reusing.

4.6. Adsorption isotherms

Adsorption isotherm describes about the adsorbate adsorbed on adsorbent surface at equilibrium at constant temperature. It gives general idea about the effectiveness of the adsorbent in removing fluoride ions from water. Analysis of the isotherm data is very important because the isotherm describe equilibrium relationship between adsorbate and adsorbent for the adsorption process. For this study, the Langmuir adsorption isotherm model and Freundlich adsorption isotherm model were used to evaluate adsorption process. These two parameter models are simple and give a good description of experimental behavior in a large range of operating conditions. The two parameter models were determined from R^2 value.

4.6.1. Langmuir Adsorption Isotherm Model

The Langmuir adsorption isotherm model works based on the assumption of a monolayer and is dependent on the assumption that the adsorbent surface consists of active sites having a uniform energy of adsorption onto the surface of adsorbent. The basic assumptions of Langmuir adsorption isotherm model are: - (i) Monolayer adsorption: adsorbate molecules are not sited in another adsorbate molecule on top. (ii) Homogeneous surface, (iii) each adsorption sites are equivalent, and (iv) there are no interactions between adsorbate molecules on adjacent sites.

Langmuir adsorption isotherm model was expressed by (Equation 11):

Langmuir isotherm linear equation: $\frac{1}{q_e} = \frac{1}{bQ_{max}c_e} + \frac{1}{Q_{max}}$ ……..... (11)

Where Ce (mg/L) is the equilibrium concentration of the adsorbate, qe (mg/g) is the amount of adsorbate per unit mass of adsorbent, Q_{max} (mg/g) and b (L/mg) are Langmuir constant related to represents monolayer maximum adsorption capacity when the homogeneous surfaces are covered with adsorbed species having uniform energies of adsorption and rate of adsorption, respectively. When the value of Langmuir constant (b) is relatively larger it indicates that there is a strong interaction between adsorbate and adsorbent while smaller value implies a weak interaction.

Table 10: Langmuir's adsorption isotherm data

Initial Concentration (Co) in mg/L	Final Concentration (Ce) in mg/L	qe in mg/g	Ce/qe	LogCe	Logqe
10	0.2	0.70	0.286	- 0.699	- 0.1549
15	0.6	1.029	0.583	- 0.2218	0.0124
20	1.09	1.35	0.807	0.0374	0.1303
25	1.82	1.656	1.099	0.26	0.219

Adsorption capacity (qe) described the fluoride uptake capacity by unit mass of an adsorbent. From (Table 10) at low concentration (10 mg/L) the adsorption capacity is 0.7 mg/g, while at high concentration (25 mg/L) the adsorption capacity is 1.656 mg/g. This shows that as concentration increases adsorption capacity increases.

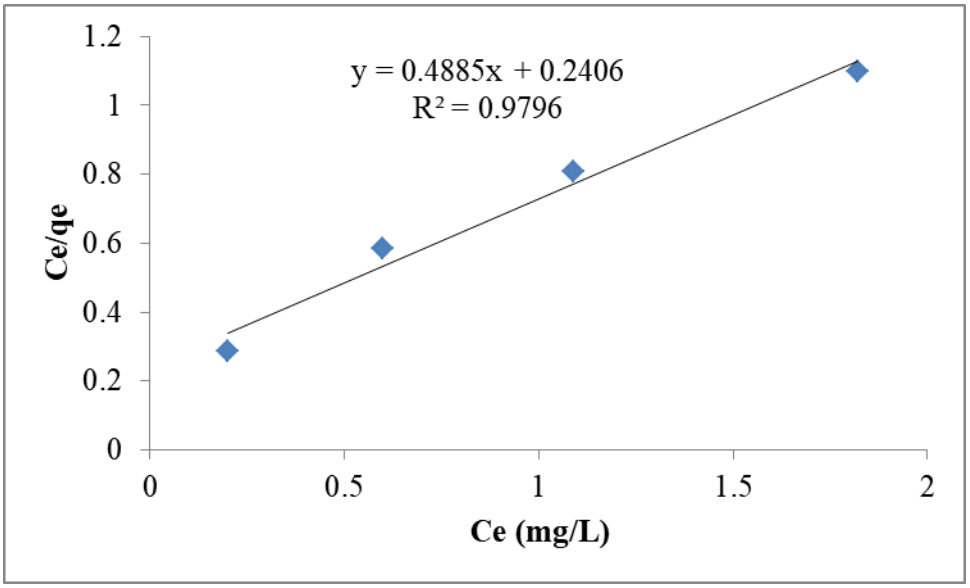

Figure 8: Linearized Langmuir adsorption isotherm concentration versus ratio of concentration to adsorption capacity for fluoride adsorption.

The Langmuir constants Q_{max} and b was determined from the slope of plotted graph and intercept of the plotted graph. That is $\frac{1}{bQ_{max}}$ is the slope and $\frac{1}{Q_{max}}$ is an intercept of the plot graph. From (Figure 8) the value of correlation coefficient ($R^{2)}$, Langmuir constant related to maximum adsorption capacity and rate of adsorption were calculated 0.9796, 4.2 mg/g and 0.49 L/mg, respectively. The result 4.2 mg/g of Q_{max} indicated that the maximum adsorption capacity for this adsorbent is 4.2 mg/g even when there was competition from the other commonly occurring anions. The small result 0.49 L/mg rate of adsorption (b) indicated that there is weak interaction between adsorbate and adsorbent. The Langmuir isotherm can be explained by a dimensionless separation factor (RL) (Equation 12).

$$RL = \frac{1}{1+bC_o} \quad \text{..... (12)}$$

Where Co is the initial fluoride concentration and b is Langmuir constant.

Table 11: The values of RL for fluoride adsorption by $Fe_{0.05}$HAp

Initial fluoride concentration (mg/L)	RL
10	0.1694
15	0.1197
20	0.0926
25	0.0755

From the initial fluoride concentration the value of RL was calculated and found to be between 0 and 1 (0.1694 - 0.0755). The value of RL indicates the type of isotherm to be either irreversible (RL = 0), favorable (0 < RL< 1), unfavorable (RL > 1), linear (RL = 1). Depending on the RL values the adsorption of fluoride on the adsorbent under the experimental condition is favorable.

4.6.2. Freundlich Adsorption Isotherm Model

The equilibrium data were analyzed using the Freundlich adsorption isotherm model. Freundlich-type adsorption is considered to be a multilayer process in which the amount of adsorbed solute per unit adsorbent mass increases gradually. The Freundlich adsorption isotherm model equation takes into account repulsive interactions between adsorbed solute particles and also accounts for surface heterogeneities. Freundlich adsorption isotherm model is expressed by (Equation 13).

Freundlich isotherm linear equation: $\log qe = \frac{1}{n} \log Ce + \log K$ ……..... (13)

Where Ce (mg/L) is the equilibrium concentration of the adsorbate, qe (mg/g) is the amount of adsorbate per unit mass of adsorbent, K and n are Freundlich constant, and 1/n is the adsorption capacity of the adsorbent. The value of K and n are calculated from the intercept and slope of the straight line of the plotted graph log Ce versus log qe. The graph of log Ce versus log qe was plotted by using the result of log Ce and log qe in (Table 10).

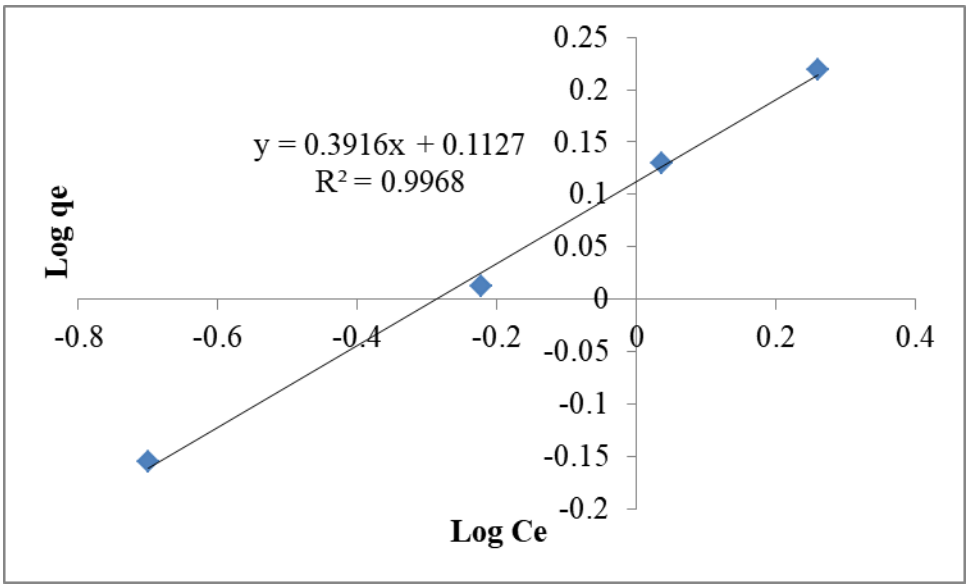

Figure 9: Freundlich adsorption isotherm log Ce versus log qe for fluoride adsorption.

From (Figure 9) the value of Freundlich constant and adsorption capacity of the adsorbent was calculated. The value of 1/n is the slope and log K is an intercept of the plotted graph. The smaller value of K (1.3) represents a smaller adsorption capacity. The adsorption intensity of n values (2.55) lying between 1 and 10.

Depending on n values it can be concluded that the adsorption of fluoride on the adsorbent under the experimental condition is favorable adsorption process. Correlation coefficients (R^2) values are used to determine whether the adsorption process follows Freundlich model or Langmuir isotherm model. (Figures 8-9) show that the values of R^2 were 0.9796 and 0.9968 Langmuir isotherm model and Freundlich isotherm model, respectively. The R^2 of Freundlich isotherm model is greater than the Langmuir isotherm model. This indicated that the adsorption was multilayer adsorption on the structurally heterogeneous surface of the Fe-HAp in the fluoride removal process. The R^2 value of Langmuir isotherm model is unacceptability model, because the correlation coefficient ($R^2 < 0.980$). Adsorption data fitted well in linearized form of model equation ($R^2 > 0.980$), which indicated the acceptability of the model (Kanaujia et al., 2015).

4.7. Adsorption Kinetic Models

An investigation of the mechanism of adsorption process and its potential rate controlling steps that include mass transfer and chemical reaction processes, adsorption kinetic models are exploited to test the experimental data. Adsorption kinetic model is the measure of the adsorption uptake with respect to time at a constant concentration and is employed to measure the diffusion of adsorbate into on the adsorbent surface and in the pores of the adsorbent. The adsorption kinetic model experiments were carried out by using different contact times (1 hr, 3 hr, 5 hr and 7 hr) with other constant parameters like adsorbent dose 0.7 g and pH 3. Also the adsorption kinetics was studied with initial fluoride concentration 10, 15, 20 and 25 mg/L. The kinetics study of fluoride adsorption was analyzed by pseudo first order and pseudo second order models. Pseudo first order kinetic model described that the speed of occupation of adsorption sites is proportional to the number of unoccupied sites on the adsorbent surface. The pseudo second order kinetic model is based on the assumption that the rate limiting step is chemical adsorption and predicts the properties over the whole range of adsorption process. Pseudo first order and pseudo second order kinetics were expressed by (Equation 14 and 15).

Pseudo first order kinetics model: $\log (qe - qt) = \log qe - \frac{k_1}{2.303} t$ ..... (14)

Pseudo second order kinetic model: $\frac{t}{qt} = \frac{1}{k_2 qe^2} + \frac{t}{qe}$ ..... (15)

Where pseudo first order constant (K_1), pseudo second order constant (K_2), equilibrium adsorption capacity (qe) and equilibrium adsorption capacity at a given t (qt). K_1, K_2 and qe can be determined from the slope and intercept of plotted graph log (qe- qt) versus t, and t/qt versus t, respectively. Logqe is the intercept and $-k_1$ is the slope for pseudo first order kinetics. $\frac{1}{K_2 q_e^2}$ is the intercept and 1/qe is the slope for pseudo second order kinetics.

Table 12: pseudo first order and pseudo second order kinetics models Parameters.

Initial concentration mg/L	Contact time (min)	qe mg/g	qt mg/g	Log (qe-qt)	$\frac{t}{q_t}$
10	60	0.70	0.66	-1.398	90.91
15	180	1.029	0.7	- 0.4828	257.14
20	300	1.35	0.69	- 0.1804	434.78
25	420	1.656	0.65	0.0026	646.15

a)

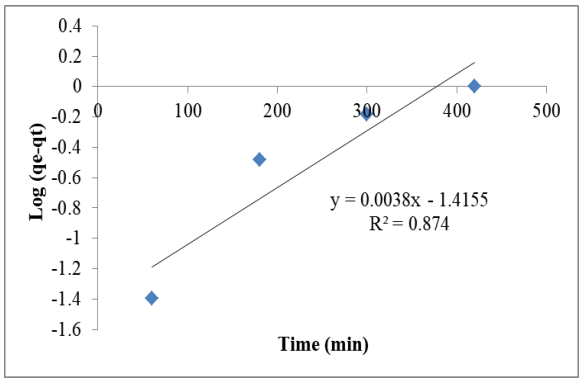

b)

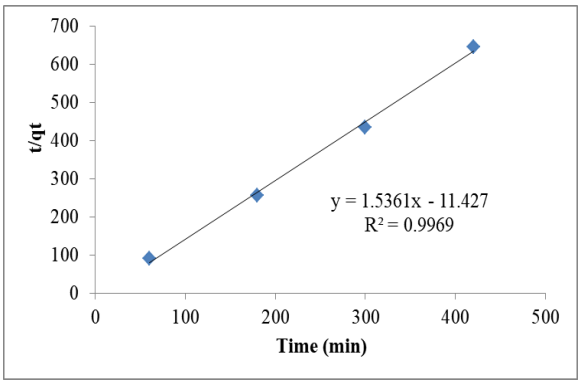

Figure 10: Result of kinetics model (a) pseudo first order kinetic model and (b) pseudo second order kinetic model

Table 13: Pseudo first order and pseudo-second-order kinetic constants model parameters

Pseudo first order					Pseudo second order				
Slope	Intercept	K_1 (min^{-1})	qe cal. (mg/g)	R^2	Slope	Intercept	K_2 (g/min mg)	qe cal. (mg/g)	R^2
0.0038	-1.4155	0.0088	0.0384	0.874	1.5361	-11.427	0.21	0.65	0.9969

Pseudo first order and pseudo second order constant (Table 13) were calculated using (Equations 12 and 13). Depending on correlation coefficient (R^2) the kinetics models were determined. (Figures 10) shows that the values of correlation coefficient (R^2) were 0.874 and 0.9969 pseudo first order kinetics and pseudo second order kinetics, respectively. The R^2 of pseudo second order kinetics is greater than pseudo first order kinetics. This indicated that an experimental data of the present study best fits to the pseudo second order kinetics. Also the value of pseudo first order rate constant K_1 and the value of pseudo second order rate constant K_2 was described adsorption kinetics. There is small adsorption rate constant K_1 and also the value of $K_1 < K_2$; this indicates that adsorption kinetics was slower adsorption rate. Larger adsorption rate constant K_1 usually represents a quicker adsorption rate while larger values of adsorption rate constant K_2 represent a slower adsorption rate (Getachew et al., 2015).

4.8. Antibacterial Activity

Synthesized HAp_4 and $Fe_{0.05}HAp$ were evaluated on antibacterial activity against gram negative *E.coli* ATCC 25922 bacteria and gram positive *S. aureus* ATCC 25923 bacteria. Contrimoxazole was taken as the standard (positive control) for all bacterial strains and DMSO was taken as negative control. Four different concentrations (3.73 mg/L, 7.5 mg/L, 15 mg/L and 30 mg/L) were prepared for studying the antibacterial activity. All concentration can be used on one plate for one bacteria species during evaluation of antibacterial activity. The evaluation of synthesized HAp and $Fe_{0.05}HAp$ on antibacterial activity test against the *E. coli* ATCC 25922 bacteria and *S.aureus* ATCC 25923 bacteria were recorded in (Table 14).

Table 14: Antibacterial efficiency of HAp_4 and $Fe_{0.05}HAp$ by different concentration

Types of sample and organism			Diameter of Zone of inhibition observed at different concentration of samples in mm					
No	Types of sample	Types of bacteria	3.75 mg/mL (D)	7.5 mg/mL (C)	15 mg/mL (B)	30 mg/mL (A)	Contrimoxazole (+ ve)	DMSO (- ve)
1	HAp_4	*E.Coli* ATCC 25922	9	10	11	11	21	6
		S.aureus ATCC 25923	6.5	7	8	8	22	6
2	$Fe_{0.05}HAp$	*E.Coli* ATCC 25922	7	9	10	11	21	6
		S.aureus ATCC 25923	6	6	6	6	23	6

From (Table 14) the largest inhibition zones were recorded with 15 and 30 mg/ mL concentration gram negative bacteria *E.coli* ATCC 25922 (11 mm) and gram-positive bacteria *S. aureus* ATCC 25923 (8 mm). The lowest inhibition zones were recorded with 3.75 mg/ mL gram negative bacteria *E.coli* ATCC 25922 (9 mm) and gram-positive bacteria *S. aureus* ATCC 25923 (6.5 mm). At 3.75 mg/mL concentration the inhibition zone of negative control and the inhibition zone of gram-positive bacteria *S. aureus* ATCC 25923 had closely diameter. This shows that at lower concentration of pure HAp_4 had low inhibition zone of *S. aureus* ATCC 25923 bacteria.

When synthesized HAp_4 compared with standard drug (Contrimoxazole), Contrimoxazole have the greatest inhibition effect against both bacteria rather than synthesized HAp_4, the control solvents (DMSO) has no inhibition zone and showed no effect to the test solutions. Table 14 shows that the bacterial growth decreases as concentration of HAp_4 increases. As it is shown in (Table 14) HAp_4 is more inhibitory gram-negative bacteria *E.coli* ATCC 25922 than gram-positive bacteria *S. aureus* ATCC 25923. This is due to the cell wall attributes differ between gram-negative *E. coli* ATCC 25922 and gram-positive *S. aureus* ATCC 25923 bacteria. *E. coli* ATCC 25922 has a relatively thin cell wall made of peptidoglycans while *S. aureus* ATCC 25923 has a relatively thick cell wall made of large amount of mucopeptides (Ragab et al., 2014). The permeability of Ca^{2+} ions of HAp is more in gram-negative bacteria due to thin cell walls. Ca^{2+} ions showed their effect on the oxygen consumed by the bacteria along with the production of free oxidative radicals that caused damage of cell membrane of the bacteria (Tejaswini et al., 2020). The Gram-positive *S. aureus* ATCC 25923 bacteria are less susceptible to Ca^{2+} ions than Gram-negative *E. coli* ATCC 25922 bacteria due to differences in their membrane structure and have thicker cell wall (Ragab et al., 2014).

From (Table 14) the largest inhibition zones were recorded with 30 mg/ mL concentration against *E.coli* ATCC 25922 (11 mm) and the lowest inhibition zones were recorded with 3.75 mg/ mL against *E.coli* ATCC 25922 (7 mm). As concentration of $Fe_{0.05}HAp$ increases, the inhibition zone of *E.Coli* ATCC 25922 bacteria increase. The inhibition zone reflects the bacteria sensibility to toxic agents so that the disinfectant-sensitive strains show large inhibition diameter and the resistant strains show a smaller or zero inhibition diameter. Figure 12 shows that at largest and lowest concentration of $Fe_{0.05}HAp$ no inhibition zone against bacteria S. aureus ATCC 25923 was observed. The inhibition zone of negative control (DMSO) and inhibition zone of sample was equal in diameter. The thick cell wall of gram-positive bacteria S.aureus resists antibacterial agents. The synthesized HAp_4 and $Fe_{0.05}HAp$ was already the same inhibition zone of gram negative bacteria. Also the synthesized HAp_4 was effective on gram positive bacteria, while $Fe_{0.05}HAp$ was not effective on gram positive bacteria. In generally, $Fe_{0.05}HAp$ is not effective for antibacterial activity, due to the same inhibition zone was observed.

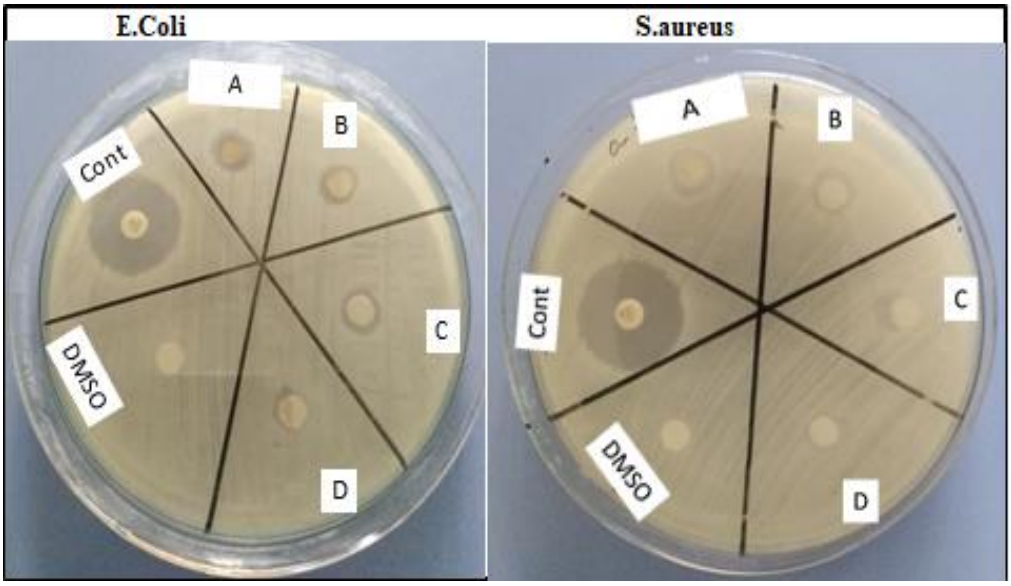

Figure 11: Antibacterial activity of HAp_4 at different concentrations against E.coli ATCC 25922 and S.aureus ATCC 25923.

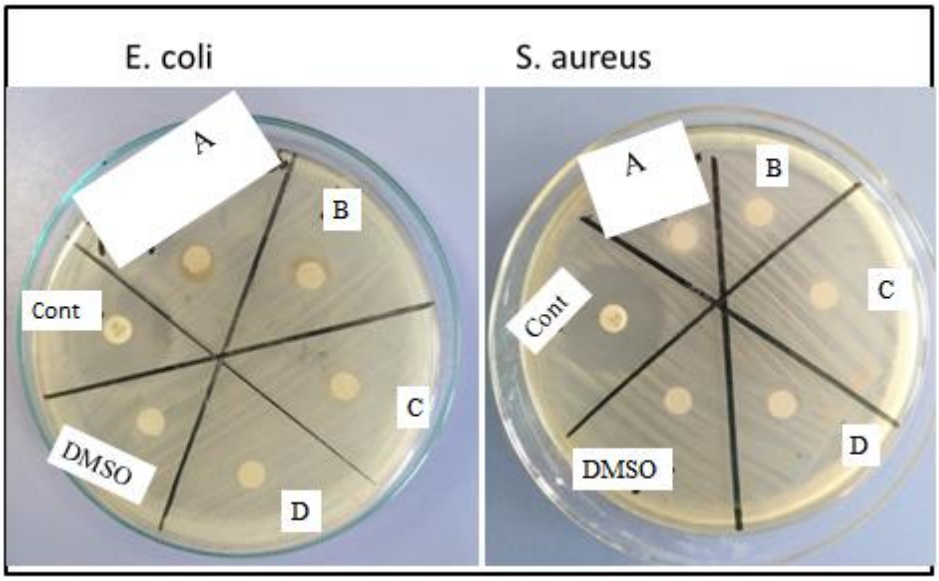

Figure 12: Antibacterial activity of $Fe_{0.05}HAp$ at different concentration against E.coli and S.aureus

Figure 11 and 12 illustrates photographs of the antibacterial tests results of synthesized HAp_4 and $Fe_{0.05}HAp$ and the details are summarized in (Table14). The presence of an inhibition zone indicates the antibacterial effect of the HAp_4 and $Fe_{0.05}HAp$.

4.9. Characterization of Adsorbent

4.9.1. Thermogravimetric Analysis and Differential thermal analysis

The thermal analysis of synthesized HAp_4 was investigated by TGA/ DTA analytical technique. TGA curve shows mass loss of the sample, whereas the DTA curve indicates the energy gain or loss during the process. Synthesized HAp_4 TGA analysis was measured from 31.26 ℃ to 800 ℃ at the heating rate 20 ℃/min with a constant supply of non-stop glide of nitrogen.

The TGA curves of the synthesized HAp_4 presents a total weight loss of about 4.41 mg (44.1 %) with occurring in three inflection points. The three inflection points were the evaporation of absorbed water, dehydration of hydroxides, removal of ammonia and removal of carbonate. As (Figure 13) shows that from 31.26 ℃ to 200.63 ℃, 0.539 mg (5.39 %) weight loss was observed, this indicate that evaporation of absorbed water. From 200.63 ℃ to 445.64 ℃, 3.84 mg (38.4 %) weight loss was observed, this indicate that removal of ammonia, carbonate and decomposition of HPO_4^{2-} to $P_2O_7^{4-}$ and H_2O, and removal of interstitial H_2O. From 445.64 ℃ to 700 ℃, 0.031 mg (0.31 %) a slight weight loss was observed, this indicate that decomposition of HPO_4^{2-} and removal of interstitial water molecule. (Figure 13) DTA curve shows that all peaks are endothermic peaks. After 700 ℃ the synthesized HAp could be decomposed to β-tricalcium phosphate (β-HAp).

The TGA/DTA curves of the synthesized $Fe_{0.05}HAp$ analysis in the range of 23.79 ℃ to 1001.71 ℃ at the heating rate 20 ℃/ min with a constant supply of nonstop glide of nitrogen. The TGA curves of the synthesized $Fe_{0.05}HAp$ presents a total weight loss of about 10.71 mg (88.63 %) with occurring in three inflection points. (Figure 14) shows that 0.59 mg (4.88 %) weight loss was observed from 23.79 ℃ to170.52 ℃, this indicate that evaporation of adsorbed water. 9.16 mg (75.81 %) weight loss was observed from 170.52 ℃ to 364.33 ℃, this indicate that removal of ammonia, carbonate and decomposition of HPO_4^{2-} to $P_2O_7^{4-}$ and H_2O, and removal of interstitial H_2O. Also 0.96 mg (7.94 %) weight loss was observed from 364.33 ℃ to 700 ℃, this indicate that decomposition of HPO_4^{2-} and removal of interstitial water molecule. From (Figure 14) DTA curve shows that at 230 ℃ the removal of ammonia gas. (Figure 14) DTA curve shows that the reaction at 558.06 ℃ was released energy, this is due to exothermic peak was observed. An exothermic peak appeared at 558.06 ℃ could be attributed to the further lattice dehydration and crystallization of $Fe_{0.05}HAp$ which indicates a reorganization in the structure.

The DTA curve of HAp_4 there is no exothermic peak was observed but the DTA curve of $Fe_{0.05}HAp$ there is exothermic peak was observed. From TGA analysis there is no weight loss after 700 ℃. As temperature of calcination increase above 700 ℃ the synthesized HAp_4 and $Fe_{0.05}HAp$ were decomposed to β-tricalcium phosphate (β-HAp) and also gradually decomposed to α-tricalcium phosphate (α-HAp).

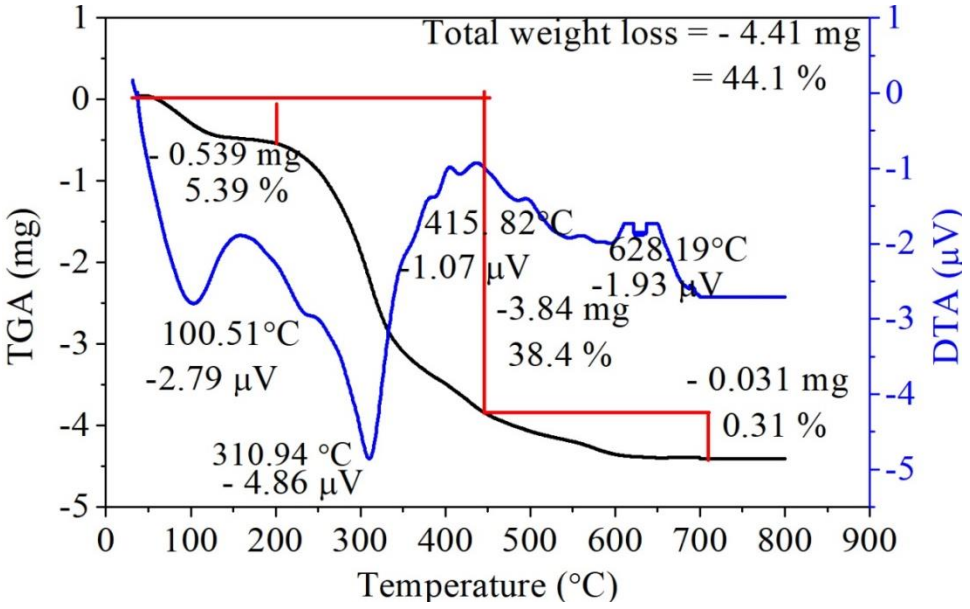

Figure 13: The result of TGA and DTA analysis of HAp_4

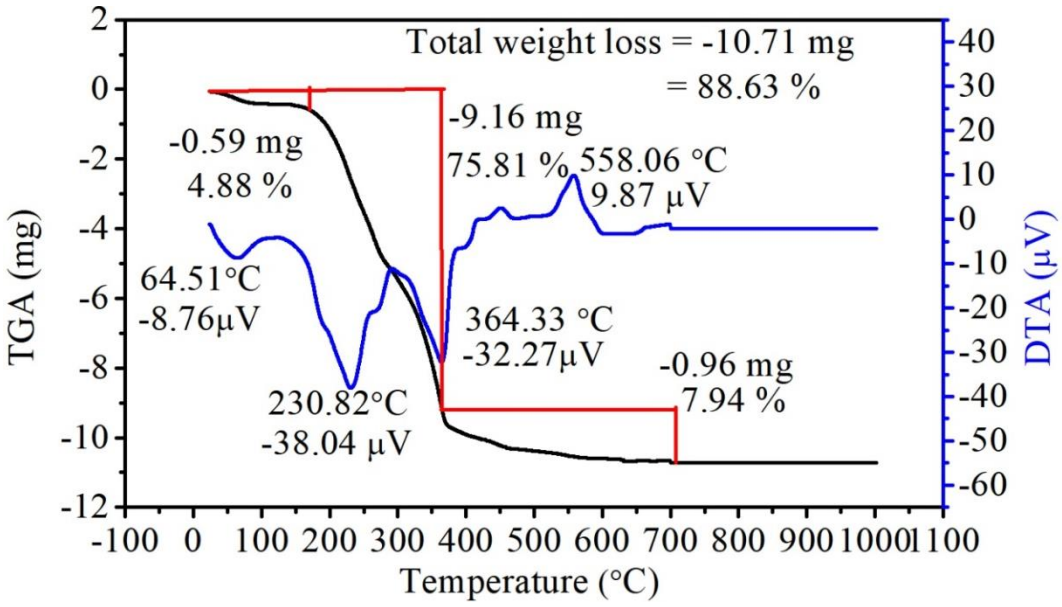

Figure 14: The result of TGA and DTA analysis of $Fe_{0.05}HAp$

4.9.2. X–ray diffraction analysis result

Crystalline structure, miller indices and space group of synthesized HAp_4 and $Fe_{0.05}HAp$ were characterized using XRD patterns. Figure 15 shows the XRD spectra of HAp_4 and $Fe_{0.05}HAp$ synthesized using 4:1 urea mass to calcium precursor mass ratio and mole of iron at x=0.05. For HAp_4 diffraction peaks were observed at 2θ values, 26.12º, 31.14º, 32.16º and 34.46º which corresponds to (002), (211), (112), and (202) plane which confirm the formation of HAp, respectively. All the XRD peaks of synthesized HAp_4 showed hexagonal phase and the observed peaks were fitted with the standard (JCPDS card No. 00-009-0432, space group P63/m). Also the diffraction peaks of $Fe_{0.05}HAp$ observed at 2θ positions 26.16º (002), 31.7º (211), 32.2º (112), 34.72º (202) shows the formation similar crystallized hexagonal hydroxyapatite structure, similar result was reported by (Kabir et al., 2012). Fe-HAp undergoes important local geometry reorganization. Since Fe^{3+} has a smaller ionic radius than Ca^{2+}, it shifts to adjacent orthophosphate (PO_4^{3-}) groups. To retain sufficient coordination, Fe^{3+} ion slightly rotates the PO_4^{3-} groups and attracts an additional oxygen atom, which could be from OH group. The Fe^{3+} forms the shortest bond with oxygen from the closest hydroxyl (releasing H^+). The Fe…O distance bond is smaller than Ca…O distance bond (Goldberg et al., 2021). During shift of peak was appeared an interstitial defect of Ca^{2+} ion site is formed due to Fe^{3+} ions substitute Ca^{2+} ions. This is due to every two Fe^{3+} ions could be substitute with three Ca^{2+} ions to provide the ionic balance (Kaygili, 2019).

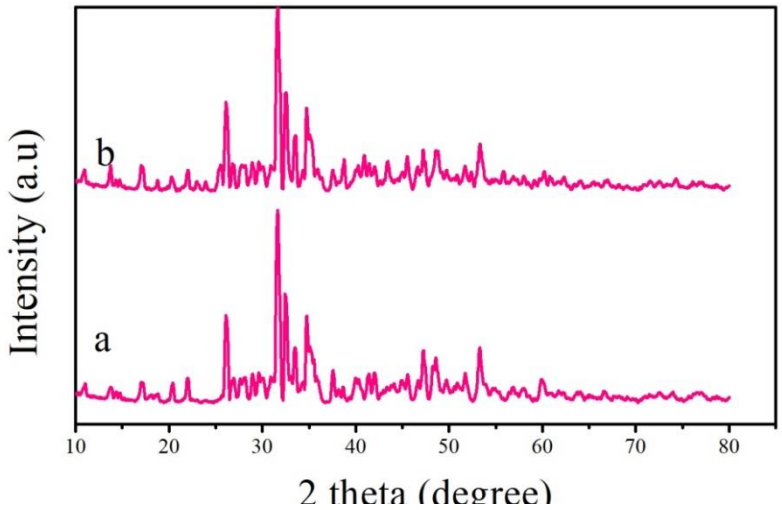

Figure 15: Result of X-ray Diffraction a) HAp_4 and b) $Fe_{0.05}HAp$

The crystallite size and average crystallite size of the synthesized HAp_4 and $Fe_{0.05}HAp$ powders were determined from the four broadening peak. The Scherer's formula was used to calculate the crystal size from the XRD spectra as given in (Equation 16).

$$D = \frac{k\lambda}{\beta\cos_{\theta}} \quad \text{..... (16)}$$

Where, D is the crystallite size (nm), k is the Scherer constant (0.94 for spherical hexagonal structure), λ is the wavelength of the X-ray radiation (0.15406 nm), and β is the experimental full width at half maximum intensity of the diffraction peak under the consideration peak; θ is the diffraction angle (degree). The crystallite size of HAp_4 was 32.54 nm and the crystallite size of $Fe_{0.05}HAp$ was 27.91 nm. This finding is in good agreement with the findings of a result reported by (Kaygili et al., 2014). This indicated that the addition of Fe into HAp_4 decreases the crystallite size. This is due to the ionic radius of Fe^{3+} (0.064 nm) is smaller than that of Ca^{2+} (0.099 nm). For the addition of Fe into HAp_4, it can be assumed that every two Fe^{3+} ions substitute with three Ca^{2+} ions to arrange for the ionic balance (Kaygili, 2019).

Table 15: Crystallite size and average crystallite size of HAp_4 and $Fe_{0.05}HAp$

Types of sample	2theta (degree)	Cosθ	β(rad)	K	λ(nm)	Crystallite Size	Average crystallite size
HAp_4	26.12	0.9741	0.0042	0.94	0.15406	35.4	32.54 nm
	31.14	0.9633	0.00548	0.94	0.15406	27.43	
	32.16	0.9609	0.00506	0.94	0.15406	29.78	
	34.46	0.9551	0.00404	0.94	0.15406	37.53	
$Fe_{0.05}HAp$	26.16	0.9741	0.005102	0.94	0.15406	29.14	27.91 nm
	31.7	0.962	0.006074	0.94	0.15406	24.78	
	32.2	0.9608	0.00543	0.94	0.15406	27.8	
	34.72	0.9544	0.00508	0.94	0.15406	29.9	

The interplanar spacing and lattice parameters both were described the properties of the synthesized material. The interplanar spacing is the perpendicular spacing between the parallel planes (hkl). The interplanar spacing and lattice parameters of HAp_4 and $Fe_{0.05}HAp$ were calculated by using major peaks. Interplanar spacing and lattice parameters of hexagonal structure of HAp_4 and $Fe_{0.05}HAp$ can be calculated by (Equations 17 and 18).

$$d = \frac{n\lambda}{2\sin_\theta} \quad \ldots\ldots (17)$$

$$\frac{1}{d^2{}_{hkl}} = \frac{4}{3a^2}\,(h^2 + hk + k^2\;) + \frac{l^2}{c^2} \quad \ldots\ldots (18)$$

Where, d-spacing interplanar (nm), θ Peak position, λ is X-ray wavelength (0.15406 nm), n order of diffraction (1), D is crystallite size (nm), lattice parameters (nm).

The lattice parameters (a-c) were calculated from the two miller indices (300) and (002) planes corresponding to peak position 33.1º and 26.12º, respectively. For the first miller indices the value of h =3, k and l = 0. For the second miller indices the value of l = 2, h and k = 0. For HAp_4 lattice constant: a = $2d_{300}\sqrt{3}$, a = 0.940 nm, c = $2d_{002}$, c = 0.6818 nm. For $Fe_{0.05}$HAp lattice constant: a = 0.934 nm, c = 0.6806 nm. From the calculation the lattice constant (a-c) decreases from 0.940 nm to 0.934 nm, 0.6818 nm to 0.6806 nm, respectively. The lattice parameters slightly decreased as the Fe^{3+} was introduced due to the difference in the ionic radii of Fe^{3+} (0.064 nm) compared to ionic radii Ca^{2+} (0.099 nm) (Goldberg et al., 2021). The substitution of ionic radii of Ca^{2+} ions by the smaller ionic radii of Fe^{3+} ions led to a greater decrease in the parameter a compared to parameter c.

Table 16: d-spacing interplaner and Lattice parameters were determined from the major peaks of HAp_4 and $Fe_{0.05}HAp$.

Types of samples	2 theta	Theta	2sinθ	d-spacing (nm)	λ (nm)	Lattice parameters	
						a (nm)	c (nm)
HAp_4	26.12	13.06	0.4519	0.3409	0.15406		0.6818
	31.14	15.57	0.5368	0.287	0.15406		
	32.16	16.08	0.5539	0.278	0.15406		
	33.02	16.51	0.5683	0.2711	0.15406	0.940	
	34.46	17.23	0.5924	0.260	0.15406		
$Fe_{0.05}HAp$	26.16	13.08	0.4526	0.3403	0.15406		0.6806
	31.7	15.85	0.5462	0.282	0.15406		
	32.2	16.1	0.5546	0.278	0.15406		
	33.1	16.55	0.5697	0.2704	0.15406	0.937	
	34.72	17.36	0.5967	0.258	0.15406		

4.9.3. Fourier-Transform Infrared Spectroscopy

The functional group and additional impurities were characterized by Fourier-Transform Infrared Spectroscopy. The functional groups of HAp_4 and $Fe_{0.05}HAp$ compositions $Ca_{10-x}Fe_x(PO_4)_6(OH)_2$ at x= 0.05 were characterized using FT-IR spectra in the range 4000 - 400 cm^{-1}. Figure 16 shows that the formation of hydroxyapatites clearly seen in FTIR spectra of all FTIR spectra. The vibrational frequencies were observed due to the presence of PO_4^{3-}, OH^- functional groups and lattice vibrations for HAp. There is no large shift of vibration band of $Fe_{0.05}HAp$.

From (Figure 16) there are four main absorption regions; the symmetric P-O stretching bands (900 - 1000 cm^{-1}), symmetric O-P-O bending mode (400 - 500 cm^{-1}), asymmetric P–O stretching bands (1000 – 1200 cm^{-1}) and asymmetric O-P-O bending mode (500 – 700 cm^{-1}) (Singh et al., 2018). The functional group PO_4^{3-}, absorption peak of asymmetric P–O stretching at 1026 cm^{-1} and 1135cm^{-1}, absorption peak of P–O bending at 558 cm^{-1}, absorption peak of symmetric P–O stretching vibrations at 931 cm^{-1} and absorption peak bending vibration of O-P-O at 495 cm^{-1} and 450 cm^{-1}were observed confirming the formation of the hydroxyapatite. A broad peak observed at 3437 cm^{-1} depicts the lattice vibration of OH^- stretching. The absorption peak of hydroxyl groups (OH^-) bending mode appeared at 1639 cm^{-1}, due to adsorbed water on the HAp surface. A large absorption band observed in the synthesized samples at 1639 cm^{-1} the presence of physically adsorbed water (Dardouri et al., 2017). The physically adsorbed water might be come from the solvent of water, Ca $(NO_3)_2.4H_2O$ and Fe $(NO_3)_3.9H_2O$ for the synthesized HAp_4 and $Fe_{0.05}$HAp.

The appearance of the weak absorption peak for C-O vibration bonds of carbonate ion (CO_3^{2-}) at 1457 cm^{-1} which substitute PO_4^{3-} is associated with the presence of CO_2 from the air (1500–1400 cm^{-1}). The substitution of CO_3^{2-} mainly occurred in the B- type carbonate of the HAp structure. The weak absorption bands of CO_3^{2-} that substitute PO_4^{3-} functional group shows small amount of CO_3^{2-} substitute PO_4^{3-}. Such substitution of CO_3^{2-} was responsible for the decrease of the crystallinity of the product. Carbonate ion that substitute phosphate was come from the atmosphere carbon dioxide in the dissolving, stirring, reaction and the drying processes. Also absorption peak of CO_3^{2-} at 878 cm^{-1} could be substitute of OH^-. The substitution of CO_3^{2-} mainly occurred in the A- type carbonate of the HAp structure. The Ca/P atomic ratio 1.67 was affected by small amounts of CO_3^{2-} substitute PO_4^{3-}. The very weak absorption peak at 604 and 544 cm^{-1} is characteristic of the pure beta tri-calcium phosphate (β-TCP), and they not clearly appear in HAp_4 and $Fe_{0.05}$HAp FTIR spectra.

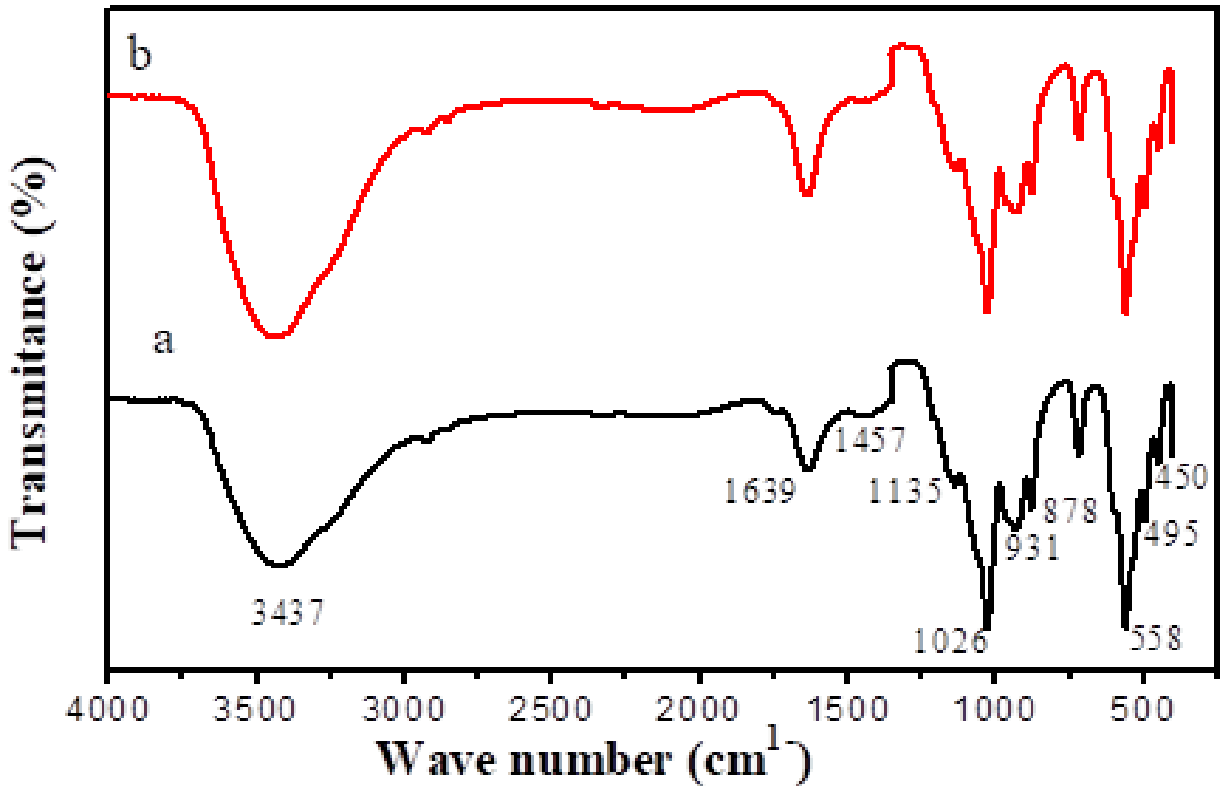

Figure 16: Result of FT-IR a) HAp_4 and b) $Fe_{0.05}HAp$

4.9.4. Scanning electron microscopy (SEM)

The surface morphology of synthesized pure HAp_4 and $Fe_{0.05}HAp$ crystals were studied using SEM image.(Figure 17a and 17b) show that the SEM images of both pure HAp4 and $Fe_{0.05}HAp$ (at x = 0.05) synthesized with urea fuel were agglomerated and without clear grain morphologies. Agglomerate is a loose arrangement of primary particles or aggregates or a mixture of the two attached, for instance, at the corners and edges. Agglomerate corresponds to the case when the dispersed particles are held together by weak physical interactions. The total surface is identical with the sum of the surfaces of the individual particles. An aggregate consists of primary particles attached at their surfaces. Aggregation is the process of formation of clusters of particles via gathering small particles by forming strong chemical bonds. The aggregation and agglomeration of nanoparticles reduces the potential enhancement of mechanical properties in nanomaterial, this is due to the restriction of interfacial area. $Fe_{0.05}HAp$ is more agglomerate than HAp_4 because the particle size and lattice parameters of nanomaterial were decreased.

$Fe_{0.05}$HAp decreases the particle size and lattice parameters, due to the ionic radius of Fe^{3+} (0.064 nm) is smaller than that of Ca^{2+} (0.099 nm) and cause agglomerate. There was also a tendency of c/a ratio decrease with a higher amount of the Fe^{3+} which will contribute to the morphology of the powders.

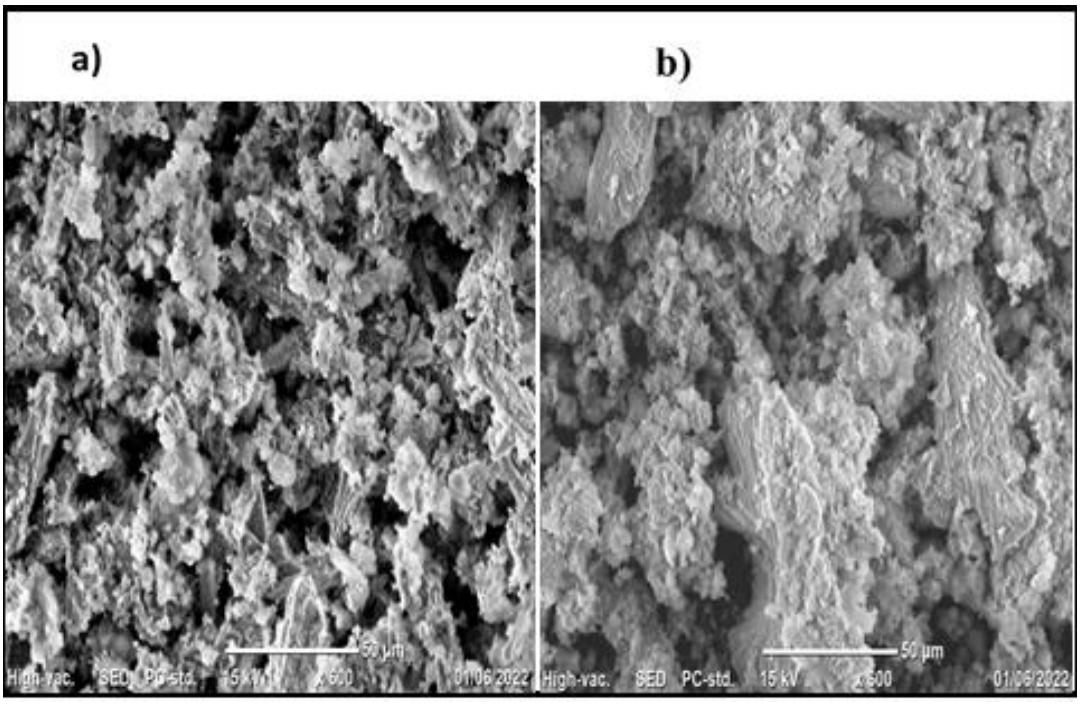

Figure 17: The SEM image a) HAp_4 b) $Fe_{0.05}$HAp.

5. CONCLUSION AND RECOMMENDATION

5.1. Conclusion

In this work Fe-HAp were synthesized from commercial chemicals through the combustion method and used for defluoridation of water by adsorption method and antibacterial activity by disc diffusion method. The adsorption data fitted well with the Freundlich adsorption isotherm models with a good correlation coefficient value which indicates multilayer adsorption on the heterogeneous adsorbent surface. The fluoride removal efficiency of $Fe_{0.05}$HAp at pH 3, 95.6 % and at pH 7, 91.1 % as measured by FISE; it shows that the adsorption of fluoride is pH dependent. The synthesized $Fe_{0.05}$HAp was applied to the ground water under optimum adsorption conditions at (contact time 3 hr, adsorbent dosage 0.7 g, pH 3, volume of solution 50 mL shaking speed 150 rpm and 6.9 mg/L of fluoride concentration of synthetic water and ground water and found to be effective with 98 % and 82.9 % fluoride removal efficiency, respectively. The maximum adsorption capacity of synthesized $Fe_{0.05}$HAp was 4.2 mg/g. The maximum inhibition zone of gram-negative bacterial strains *E. coli* ATCC 25922 11 mm was measured for HAp and $Fe_{0.05}$HAp. But there is no inhibition zone of gram-positive bacterial strains *S.aureus* ATCC 25923 was measured for $Fe_{0.05}$HAp. In generally, it concluded that $Fe_{0.05}$HAp can be employed for fluoride removal from groundwater rather than antibacterial activities.

5.2. Recommendation

Synthesis Metal doped-HAp by combustion method by using fuel is one of the emerging research areas with future prospective. Therefore, further studies may be needed for the synthesis Metal doped HAp to lower the calcinations temperature of pure and Metal doped HAp.

6. REFERENCE

Akafu, T., Chimdi, A., & Gomoro, K. (2019). Removal of Fluoride from Drinking Water by Sorption Using Diatomite Modified with Aluminum Hydroxide. *Journal of Analytical Methods in Chemistry, 2019*. https://doi.org/10.1155/2019/4831926

Ali, I., & Gupta, V. K. (2007). Advances in water treatment by adsorption technology. *Nature Protocols, 1*(6), 2661–2667. https://doi.org/10.1038/nprot.2006.370

Ayenew, T. (2008). The distribution and hydrogeological controls of fluoride in the groundwater of central Ethiopian rift and adjacent highlands. *Environmental Geology*, *54*(6), 1313–1324. https://doi.org/10.1007/s00254-007-0914-4

Ayoob, S., Gupta, A. K., & Bhat, V. T. (2008). A conceptual overview on sustainable technologies for the defluoridation of drinking water. In *Critical Reviews in Environmental Science and Technology* (Vol. 38, Issue 6). https://doi.org/10.1080/10643380701413310

Batista, H. A., Silva, F. N., Lisboa, H. M., & Costa, A. C. F. M. (2020). Modeling and optimization of combustion synthesis for hydroxyapatite production. *Ceramics International*, *46*(8), 11638–11646. https://doi.org/10.1016/j.ceramint.2020.01.194

Bensalah, H., Bekheet, M. F., Alami Younssi, S., Ouammou, M., & Gurlo, A. (2018). Hydrothermal synthesis of nanocrystalline hydroxyapatite from phosphogypsum waste. *Journal of Environmental Chemical Engineering*, *6*(1), 1347–1352. https://doi.org/10.1016/j.jece.2018.01.052

Bhatnagar, A., & Minocha, A. K. (2006). Conventional and non-conventional adsorbents for removal of pollutants from water - A review. *Indian Journal of Chemical Technology*, *13*(3), 203–217.

Bhaumik, R., & Kumar, N. (2014). Optimizing adsorption of fluoride from water by modified banana peel dust using response surface modelling approach. *Applied Water Science*, 6, 115–135. https://doi.org/10.1007/s13201-014-0211-9

Bouyer, E., Gitzhofer, F., & Boulos, M. I. (2000). Morphological study of hydroxyapatite nanocrystal suspension. *Journal of Materials Science: Materials in Medicine*, *11*(8), 523–531. https://doi.org/10.1023/A:1008918110156

Cahyaningrum, S. E., Herdyastuty, N., Devina, B., & Supangat, D. (2018). Synthesis and Characterization of Hydroxyapatite Powder by Wet Precipitation Method. *IOP Conference Series: Materials Science and Engineering*, *299*(1). https://doi.org/10.1088/1757-899X/299/1/012039

Cao, L. Y., Zhang, C. B., & Huang, J. F. (2005). Synthesis of hydroxyapatite nanoparticles in ultrasonic precipitation. *Ceramics International*, *31*(8), 1041–1044. https://doi.org/10.1016/j.ceramint.2004.11.002

Chinnakoti, P., Chunduri, A. L. A., & Vankayala, R. K. (2017). Enhanced fluoride adsorption by nano crystalline c -alumina : adsorption kinetics , isotherm modeling and thermodynamic studies. *Applied Water Science*, *7*(5), 2413–2423. https://doi.org/10.1007/s13201-016-0437

Chitra Devi, S., Narmadha, B., & Kanagavalli, C. (2020). Green Synthesis of Hydroxy Apatite Nanoparticle By Sol - Gel Method Using Papaya Leaf (Carica Papaya) and Indian Nettle Leaf (Acalypha Indica) As Solvents. *International Journal of Advanced Research*, *8*(02), 232–241. https://doi.org/10.21474/ijar01/10458

Chowdhury, S., Mishra, R., Saha, P., & Kushwaha, P. (2011). Adsorption thermodynamics, kinetics and isosteric heat of adsorption of malachite green onto chemically modified rice husk. *Desalination*, *265*(1–3), 159–168. https://doi.org/10.1016/j.desal.2010.07.047

Dadi, R., Azouani, R., Traore, M., Mielcarek, C., & Kanaev, A. (2019). Antibacterial activity of ZnO and CuO nanoparticles against gram positive and gram negative strains. *Materials Science and Engineering C*, *104*, 109968. https://doi.org/10.1016/j.msec.2019.109968

Dardouri, M., Borges, J. P., & Omrani, A. D. (2017). Tailoring the morphology of hydroxyapatite particles using a simple solvothermal route. *Ceramics International*, *43*(4), 3784–3791. https://doi.org/10.1016/j.ceramint.2016.12.022

Dhillon, A., Nair, M., Bhargava, S. K., & Kumar, D. (2015). Excellent fluoride decontamination and antibacterial efficacy of Fe-Ca-Zr hybrid metal oxide nanomaterial. *Journal of Colloid and Interface Science*, *457*, 289–297. https://doi.org/10.1016/j.jcis.2015.06.045

Ergun, E., Tor, A., Cengeloglu, Y., & Kocak, I. (2008). Electrodialytic removal of fluoride from water: Effects of process parameters and accompanying anions. *Separation and Purification Technology*, *64*(2), 147–153. https://doi.org/10.1016/j.seppur.2008.09.009

Fakharzadeh, A., Ebrahimi-Kahrizsangi, R., Nasiri-Tabrizi, B., & Jefrey Basirun, W. (2017). Effect of dopant loading on the structural features of silver-doped hydroxyapatite obtained by mechanochemical method. *Ceramics International*, *43*(15), 12588–12598. https://doi.org/10.1016/j.ceramint.2017.06.136

Getachew, T., Hussen, A., & Rao, V. M. (2015). Defluoridation of water by activated carbon prepared from banana (Musa paradisiaca) peel and coffee (Coffea arabica) husk. *International Journal of Environmental Science and Technology*, *12*(6), 1857–1866. https://doi.org/10.1007/s13762-014-0545-8

Ghorai, S., & Pant, K. K. (2005). Equilibrium, kinetics and breakthrough studies for adsorption of fluoride on activated alumina. *Separation and Purification Technology*, *42*(3), 265–271. https://doi.org/10.1016/j.seppur.2004.09.001

Ghosh, S. K., Pal, S., Roy, S. K., Pal, S. K., & Basu, D. (2010). Modelling of flame temperature of solution combustion synthesis of nanocrystalline calcium hydroxyapatite material and its parametric optimization. *Bulletin of Materials Science*, *33*(4), 339–350. https://doi.org/10.1007/s12034-010-0052-6

Ghosh, S. K., Roy, S. K., Kundu, B., Datta, S., & Basu, D. (2011). Synthesis of nano-sized hydroxyapatite powders through solution combustion route under different reaction conditions. *Materials Science and Engineering B: Solid-State Materials for Advanced Technology*, *176*(1), 14–21. https://doi.org/10.1016/j.mseb.2010.08.006

Goldberg, M. A., Gafurov, M. R., Murzakhanov, F. F., Fomin, A. S., Antonova, O. S., Khairutdinova, D. R., Pyataev, A. V., Makshakova, O. N., Konovalov, A. A., Leonov, A. V., Akhmedova, S. A., Sviridova, I. K., Sergeeva, N. S., Barinov, S. M., & Komlev, V. S. (2021). Mesoporous iron(iii)-doped hydroxyapatite nanopowders obtained via iron oxalate. *Nanomaterials*, *11*(3), 1–21. https://doi.org/10.3390/nano11030811

Govindaraj, D., & Rajan, M. (2016). ScienceDirect Synthesis and Spectral Characterization of Novel nano- Hydroxyapatite from Moringaoleifera Leaves. *Materials Today: Proceedings*, *3*(6), 2394–2398. https://doi.org/10.1016/j.matpr.2016.04.153

Habuda-Stanić, M., Ravančić, M., & Flanagan, A. (2014). A Review on Adsorption of Fluoride from Aqueous Solution. *Materials*, *7*(9), 6317–6366. https://doi.org/10.3390/ma7096317

Hadagalli, K., Shenoy, S., Shakya, K. R., Manjunath, G., Tarafder, K., Mandal, S., & Basu, B. (2021). Effect of Fe^{3+} substitution on the structural modification and band structure modulated UV absorption of hydroxyapatite. *International Journal of Applied Ceramic Technology*, *18*(2), 332–344. https://doi.org/10.1111/ijac.13674

Haider, A., Haider, S., Han, S. S., & Kang, I. K. (2017). Recent advances in the synthesis, functionalization and biomedical applications of hydroxyapatite: a review. *RSC Advances*, *7*(13), 7442–7458. https://doi.org/10.1039/c6ra26124h

Han, Y., Li, S., Wang, X., & Chen, X. (2004). Synthesis and sintering of nanocrystalline hydroxyapatite powders by citric acid sol-gel combustion method. *Materials Research Bulletin*, *39*(1), 25–32. https://doi.org/10.1016/j.materresbull.2003.09.022

He, J., Zhang, K., Wu, S., Cai, X., Chen, K., Li, Y., Sun, B., Jia, Y., Meng, F., Jin, Z., Kong, L., & Liu, J. (2016). Performance of novel hydroxyapatite nanowires in treatment of fluoride contaminated water. In *Journal of Hazardous Materials* (Vol. 303). Elsevier B.V. https://doi.org/10.1016/j.jhazmat.2015.10.028

Hoai, T. T., Nga, N. K., Giang, L. T., Huy, T. Q., Tuan, P. N. M., & Binh, B. T. T. (2017). Hydrothermal Synthesis of Hydroxyapatite Nanorods for Rapid Formation of Bone-Like Mineralization. *Journal of Electronic Materials*, *46*(8), 5064–5072. https://doi.org/10.1007/s11664-017-5509-6

Ismail, N. F., Hamzah, S., Razali, N. A., Yussof, W. M. H. W., Ali, N., & Mohammad, A. W. (2019). Preparation and characterisation of hydroxyapatite extracted from fish scale waste for the removal of gallic acid as inhibitor in biofuel production. *Malaysian Journal of Analytical Sciences*, *23*(6), 938–949. https://doi.org/10.17576/mjas-2019-2306-03

Izuagie, A. A., Gitari, W. M., & Gumbo, J. R. (2016). Synthesis and performance evaluation of Al/Fe oxide coated diatomaceous earth in groundwater defluoridation: Towards fluorosis mitigation. *Journal of Environmental Science and Health - Part A Toxic/Hazardous Substances and Environmental Engineering*, *51*(10), 810–824. https://doi.org/10.1080/10934529.2016.1181445

Jiménez-Reyes, M., & Solache-Ríos, M. (2010). Sorption behavior of fluoride ions from aqueous solutions by hydroxyapatite. *Journal of Hazardous Materials*, *180*(1–3), 297–302. https://doi.org/10.1016/j.jhazmat.2010.04.030

Jose, S., Senthilkumar, M., Elayaraja, K., Haris, M., George, A., Raj, A. D., Sundaram, S. J., Bashir, A. K. H., Maaza, M., Kaviyarasu, K., West, S., Province, W. C., & Africa, S. (2021). Preparation and characterization of Fe doped n -hydroxyapatite for biomedical application. *Surfaces and Interfaces*, *25*(November 2020), 101185. https://doi.org/10.1016/j.surfin.2021.101185

Kabir, S. F., Ahmed, S., Mustafa, A. I., Ahsan, M., & Islam, S. (2012). Synthesis and Characterization of Fe-doped Hydroxyapatite. *Bangladesh J. Sci. Ind. Res.* 47(1), 1-8. https://doi.org/10.3329/bjsir.v47i1.10711

Kanaujia, S., Singh, B., & Singh, S. K. (2015). Removal of Fluoride from Groundwater by Carbonised <i>Punica granatum</i> Carbon (“CPGC”) Bio-Adsorbent. *Journal of Geoscience and Environment Protection*, *03*(04), 1–9. https://doi.org/10.4236/gep.2015.34001

Kanno, C. M., Sanders, R. L., Flynn, S. M., Lessard, G., & Myneni, S. C. B. (2014). *Novel Apatite-Based Sorbent for De fl uoridation: Synthesis and Sorption Characteristics of Nano-micro-crystalline Hydroxyapatite- Coated-Limestone*. *Environ. Sci. Technol.* 48(10) 5798–5807.https://doi.org/10.1021/es405135r

Kanrar, S., Debnath, S., De, P., Parashar, K., Pillay, K., Sasikumar, P., & Ghosh, U. C. (2016). Preparation, characterization and evaluation of fluoride adsorption efficiency from water of iron-aluminium oxide-graphene oxide composite material. *Chemical Engineering Journal*, *306*, 269–279. https://doi.org/10.1016/j.cej.2016.07.037

Kaygili, O. (2019). Combustion synthesis and characterization of Mg - based Fe - doped biphasic calcium phosphate ceramics. *Applied Physics A*, 1–7. https://doi.org/10.1007/s00339-019-2728-0

Kaygili, O., Dorozhkin, S. V., Ates, T., Al-Ghamdi, A. A., & Yakuphanoglu, F. (2014). Dielectric properties of Fe doped hydroxyapatite prepared by sol-gel method. *Ceramics International*, *40*(7 PART A), 9395–9402. https://doi.org/10.1016/j.ceramint.2014.02.009

Koumoulidis, G. C., Katsoulidis, A. P., Ladavos, A. K., Pomonis, P. J., Trapalis, C. C., Sdoukos, A. T., & Vaimakis, T. C. (2003). Preparation of hydroxyapatite via microemulsion route. *Journal of Colloid and Interface Science*, *259*(2), 254–260. https://doi.org/10.1016/S0021-9797(02)00233-3

Kumar, S., & Jain, S. (2013). History, introduction, and kinetics of ion exchange materials. *Journal of Chemistry*, *2013*. https://doi.org/10.1155/2013/957647

Li, Y., Widodo, J., Lim, S., & Ooi, C. P. (2012). Synthesis and cytocompatibility of manganese (II) and iron (III) substituted hydroxyapatite nanoparticles. *Journal of Materials Science*, *47*(2), 754–763. https://doi.org/10.1007/s10853-011-5851-7

Ma, G. (2019). Three common preparation methods of hydroxyapatite. *IOP Conference Series: Materials Science and Engineering*, 688(3). https://doi.org/10.1088/1757-899X/688/3/033057

Maity, J. P., Hsu, C. M., Lin, T. J., Lee, W. C., Bhattacharya, P., Bundschuh, J., & Chen, C. Y. (2018). Removal of fluoride from water through bacterial-surfactin mediated novel hydroxyapatite nanoparticle and its efficiency assessment: Adsorption isotherm, adsorption kinetic and adsorption Thermodynamics. *Environmental Nanotechnology, Monitoring and Management*, *9*(October 2017), 18–28. https://doi.org/10.1016/j.enmm.2017.11.001

Malla, K. P., Regmi, S., Nepal, A., Bhattarai, S., Yadav, R. J., Sakurai, S., & Adhikari, R. (2020). Extraction and Characterization of Novel Natural Hydroxyapatite Bioceramic by Thermal Decomposition of Waste Ostrich Bone. *International Journal of Biomaterials*, *2020*. https://doi.org/10.1155/2020/1690178

Mbugua, M., Mbuvi, H., & Muthengia, J. (2014). Rice Husk Ash Derived Zeolite Blended with Water Hyacinth Ash for Enhanced Adsorption of Cadmium Ions. *Current World Environment*, *9*(2), 280–286. https://doi.org/10.12944/cwe.9.2.08

Medellin-castillo, N. A., Leyva-ramos, R., Padilla-ortega, E., & Perez, R. O. (2014). Adsorption capacity of bone char for removing fluoride from water solution . Role of hydroxyapatite content , adsorption mechanism and competing anions. *Journal of Industrial and Engineering Chemistry*. https://doi.org/10.1016/j.jiec.2013.12.105

Mehta, D., Mondal, P., Saharan, V. K., & George, S. (2016). Synthesis of Hydroxyapatite Nanorods for application in water defluoridation and optimization of process variables: Advantage of ultrasonication with precipitation method over conventional method. *Ultrasonics - Sonochemistry*. https://doi.org/10.1016/j.ultsonch.2016.12.035

Méndez-lozano, N., Velázquez-castillo, R., Rivera-muñoz, E. M., Bucio-galindo, L., Mondragón-galicia, G., Manzano-ramírez, A., Ángel, M., & Apátiga-castro, L. M. (2016). Crystal growth and structural analysis of hydroxyapatite nano fi bers synthesized by the hydrothermal microwave-assisted method. *Ceramics International*, *September*, 0–1. https://doi.org/10.1016/j.ceramint.2016.09.179

Morsi, M. A., & Hezma, A. E. M. (2019). Effect of iron doped hydroxyapatite nanoparticles on the structural, morphological, mechanical and magnetic properties of polylactic acid polymer. *Journal of Materials Research and Technology*, *8*(2), 2098–2106. https://doi.org/10.1016/j.jmrt.2019.01.017

Mourabet, M., Rhilassi, A. El, Boujaady, H. El, Hamri, R. El, & Taitai, A. (2012). Removal of fluoride from aqueous solution by adsorption on hydroxyapatite (HAp) using response surface methodology. *Journal of Saudi Chemical Society*, *1*. https://doi.org/10.1016/j.jscs.2012.03.003

Mukherjee, I., & Singh, U. K. (2020). Fluoride abundance and their release mechanisms in groundwater along with associated human health risks in a geologically heterogeneous semi-arid region of east India. *Microchemical Journal*, *152*, 104304. https://doi.org/10.1016/j.microc.2019.104304

Palanisamy, P. N., Agalya, A., & Sivakumar, P. (2012). Polymer composite - A potential biomaterial for the removal of reactive dye. *E-Journal of Chemistry*, *9*(4), 1823–1834. https://doi.org/10.1155/2012/518581

Panneerselvam, K., Arul, K. T., & Warrier, A. R. (2019). *Rapid adsorption of industrial pollutants using metal ion doped hydroxyapatite Rapid Adsorption of Industrial Pollutants Using Metal Ion Doped Hydroxyapatite*. *020004*(June).

Panseri, S., Cunha, C., D'Alessandro, T., Sandri, M., Giavaresi, G., Marcacci, M., Hung, C. T., & Tampieri, A. (2012). Intrinsically superparamagnetic Fe-hydroxyapatite nanoparticles positively influence osteoblast-like cell behaviour. *Journal of Nanobiotechnology*, *10*, 1–10. https://doi.org/10.1186/1477-3155-10-32

Pramanik, S., Agarwal, A. K., Rai, K. N., & Garg, A. (2007). Development of high strength hydroxyapatite by solid-state-sintering process. *Ceramics International*, *33*(3), 419–426. https://doi.org/10.1016/j.ceramint.2005.10.025

Radu, A., Radu, T., McGraw, C., Dillingham, P., Anastasova-Ivanova, S., & Diamond, D. (2013). Ion selective electrodes in environmental analysis. *Journal of the Serbian Chemical Society*, *78*(11), 1729–1761. https://doi.org/10.2298/JSC130829098R

Ragab, H. S., Ibrahim, F. A., Abdallah, F., A. Al-Ghamdi, A., El-Tantawy, F., & Yakuphanoglu, F. (2014). Synthesis and In Vitro Antibacterial Properties of Hydroxyapatite Nanoparticles. *IOSR Journal of Pharmacy and Biological Sciences*, *9*(1), 77–85. https://doi.org/10.9790/3008-09167785

Rajan, M., & Alagumuthu, G. (2013). Study of fluoride affinity by zirconium impregnated walnut shell carbon in aqueous phase: Kinetic and isotherm evaluation. *Journal of Chemistry*, *2013*. https://doi.org/10.1155/2013/235048

Sadat-Shojai, M., Khorasani, M. T., Dinpanah-Khoshdargi, E., & Jamshidi, A. (2013). Synthesis methods for nanosized hydroxyapatite with diverse structures. *Acta Biomaterialia*, *9*(8), 7591–7621. https://doi.org/10.1016/j.actbio.2013.04.012

Santos, M. H., Oliveira, M. de, Souza, L. P. de F., Mansur, H. S., & Vasconcelos, W. L. (2004). Synthesis control and characterization of hydroxyapatite prepared by wet precipitation process. *Materials Research*, *7*(4), 625–630. https://doi.org/10.1590/s1516-14392004000400017

Sarkar, G. T. A. T. S. (2015). Enhanced fluoride removal by hydroxyapatite-modified activated alumina. *International Journal of Environmental Science and Technology*, 2809–2818. https://doi.org/10.1007/s13762-014-0653-5

Shi, P., Liu, M., Fan, F., Yu, C., Lu, W., & Du, M. (2018). Characterization of natural hydroxyapatite originated from fish bone and its biocompatibility with osteoblasts. *Materials Science and Engineering C*, *90*(March), 706–712. https://doi.org/10.1016/j.msec.2018.04.026

Singh, B. (2018). Biomaterials Enhanced dielectric constant and structural transformation in Fe-doped hydroxyapatite synthesized by wet chemical method. *Journal of Materials Science*, *1*. https://doi.org/10.1007/s10853-018-2225-4

Sobczak-Kupiec, A., Drabczyk, A., Florkiewicz, W., Głąb, M., Kudłacik-Kramarczyk, S., Słota, D., Tomala, A., & Tyliszczak, B. (2021). Review of the applications of biomedical compositions containing hydroxyapatite and collagen modified by bioactive components. *Materials*, *14*(9). https://doi.org/10.3390/ma14092096

Sundaram, C. S., Viswanathan, N., & Meenakshi, S. (2008). Defluoridation chemistry of synthetic hydroxyapatite at nano scale : *Equilibrium and kinetic studies*. *Journal Hazardous Materials. 155*, 206–215. https://doi.org/10.1016/j.jhazmat.2007.11.048

Tang, Q., Duan, T., Li, P., Zhang, P., & Wu, D. (2018). Enhanced defluoridation capacity from aqueous media via hydroxyapatite decorated with carbon nanotube. *Frontiers in Chemistry*, *6*(APR). https://doi.org/10.3389/fchem.2018.00104

Tejaswini, T., Keerthana, M., Vidyavathi, M., & Kumar, R. V. S. (2020). *Design and evaluation of atorvastatin- loaded chitosan-hydroxyapatite composite bioscaffolds for wound-healing activity*. *Future Journal of Pharmaceutical Sciences*. 6:111. https://doi.org/10.1186/s43094-020-00125-y

Vijayalakshmi, U., & Rajeswari, S. (2006). Preparation and characterization of microcrystalline hydroxyapatite using sol gel method. *Trends in Biomaterials and Artificial Organs*, *19*(2), 57–62.

Volkmer, T. M., Bastos, L. L., Sousa, V. C., & Santos, L. A. (2009). Obtainment of α-tricalcium phosphate by solution combustion synthesis method using urea as combustible. *Key Engineering Materials*, *396–398*(3), 591–594. https://doi.org/10.4028/www.scientific.net/kem.396-398.591

Wambu, E. W., & Muthakia, G. K. (2011). High fluoride water in the Gilgil area of Nakuru County, kenya. *High Fluoride Water,* 44(1), 37-41. https://www.researchgate.net/publication/215769551

Wang, L., Zhang, Y., Sun, N., Sun, W., Hu, Y., & Tang, H. (2019). Precipitation Methods Using Calcium-Containing Ores for Fluoride Removal in Wastewater. *Journals Minerals*,9(9), 511; https://doi.org/10.3390/min9090511

Workeneh, K., Zereffa, E. A., & Segne, T. A. (2019). *Eggshell-Derived Nanohydroxyapatite Adsorbent for Defluoridation of Drinking Water from Bofo of Ethiopia*. *Journal of Nanomaterials,2019. https://doi.org/10.1155/2019/2458312*

Wu, G., Li, P., Feng, H., Zhang, X., & Chu, P. K. (2015). Engineering and functionalization of biomaterials via surface modification. *Journal of Materials Chemistry B*, *3*(10), 2024–2042. https://doi.org/10.1039/c4tb01934b

Xia, Y., Huang, X., Li, W., Zhang, Y., & Li, Z. (2018). Facile Defluoridation of Drinking Water by Forming Shell@Fluorapatite Nanoarray during Boiling Egg Shell. *Journal of Hazardous Materials*. https://doi.org/10.1016/j.jhazmat.2018.09.007

Xu, H., Chen, Y., & Zhang, S. F. (2011). Synthesis and characterization of microporous hydroxyapatite via hydrothermal method. *Synthesis and Reactivity in Inorganic, Metal-Organic and Nano-Metal Chemistry*, *41*(1), 31–35. https://doi.org/10.1080/15533174.2010.522672

Zaman, S. U., Khaliq, M., Zaman, U., & Muhammad, N. (2020). Overview of hydroxyapatite; composition, structure, synthesis methods and its biomedical uses Ionic liquid for biomedical applications View project Sensing and Biosensing Applications of Nanomaterials View project. *Biomedical Letters*, *6*(1), 84–99.

Zhang, H., & Darvell, B. W. (2011). Formation of hydroxyapatite whiskers by hydrothermal homogeneous precipitation using acetamide. *Journal of the American Ceramic Society*, *94*(7), 2007–2013. https://doi.org/10.1111/j.1551-2916.2010.04338.x

Zhou, H., & Lee, J. (2011). Nanoscale hydroxyapatite particles for bone tissue engineering. *Acta Biomaterialia*, *7*(7), 2769–2781. https://doi.org/10.1016/j.actbio.2011.03.019

Zhu, K., Yanagisawa, K., Shimanouchi, R., Onda, A., & Kajiyoshi, K. (2006). Preferential occupancy of metal ions in the hydroxyapatite solid solutions synthesized by hydrothermal method. *Journal of the European Ceramic Society*, *26*(4–5), 509–513. https://doi.org/10.1016/j.jeurceramsoc.2005.07.019

7. APPENDICES

In this section includes the calculation parts, table and figures which is not included in the main body or textual body of the research report.

Appendix A: Experimental data

1. Moles calculation for calcium reduced and Fe doped HAp

   i. For $Ca_{10-x}Fe_x(PO_4)_6(OH)_2$ at x=0.01 from 0.03 mole of Ca.

Mole of Fe = $\frac{0.03 \text{ mole Ca x } 0.01}{10 \text{ mole Ca}}$ = 0.00003 mole of Fe

Mole of Ca = 0.03 mole – 0.00003 mole = 0.02997 mole Ca

   ii. For $Ca_{10-x}Fe_x(PO_4)_6(OH)_2$ at x=0.03 from 0.03 mole of Ca

Mole of Fe = $\frac{0.03 \text{ mole x } 0.03}{10 \text{ mole Ca}}$ = 0.00009 mole of Fe

Mole of Ca = 0.03 mole – 0.00009 mole = 0.02991 mole Ca

   iii. For $Ca_{10-x}Fe_x(PO_4)_6(OH)_2$ at x=0.05 from 0.03 mole of Ca

Mole of Fe = $\frac{0.03 \text{ mole x } 0.05}{10 \text{ mole Ca}}$ = 0.00015 mole of Fe

Mole of Ca = 0.03 mole – 0.00015 mole = 0.02985 mole Ca

   iv. For $Ca_{10-x}Fe_x(PO_4)_6(OH)_2$ at x=0.07 from 0.03 mole of Ca

Mole of Fe = $\frac{0.03 \text{ mole x } 0.07}{10 \text{ mole Ca}}$ = 0.00021 mole of Fe

Mole of Ca = 0.03 mole – 0.00021 mole = 0.02979 mole Ca

   v. For $Ca_{10-x}Fe_x(PO_4)_6(OH)_2$ at x=0.1 from 0.03 mole of Ca

Mole of Fe = $\frac{0.03 \text{ mole x } 0.1}{10 \text{ mole Ca}}$ = 0.0003 mole of Fe

Mole of Ca = 0.03 mole – 0.0003 mole = 0.0297 mole Ca

2. Preparation of fluoride concentration for calibration

Table1: calibration standard solution

Fluoride Concentration	2 ppm	4 ppm	6 ppm	8 ppm	10 ppm
Volume of deionized water in mL	24	18	12	6	0
Volume of standard solution(10 ppm) in mL	6	12	18	24	30

3. Removal efficiency of fluoride of real water

FISE reading = - 69 mV

-69 = 57.95 X - 64.876, - 69 +64.876 = 57.95 X, X = - 4.124/57.93, X = - 0.0712

- log $[F^-]$ = - 0.0712, $[F^-] = 10^{0.0712}$, $[F^-]$ = 1.18 mg/L

% 6.9 mg/L = $\frac{(6.9\ mg/L - 1.18\ mg/L)}{6.9\ mg/L}$ x 100 = 82.9 % of real water

Adsorption capacity = $\frac{(6.9\ mg/L - 1.18\ mg/L)}{0.7\ g}$ x 0.05 L = 0.41 mg/g

Appendix B: Experimental Picture

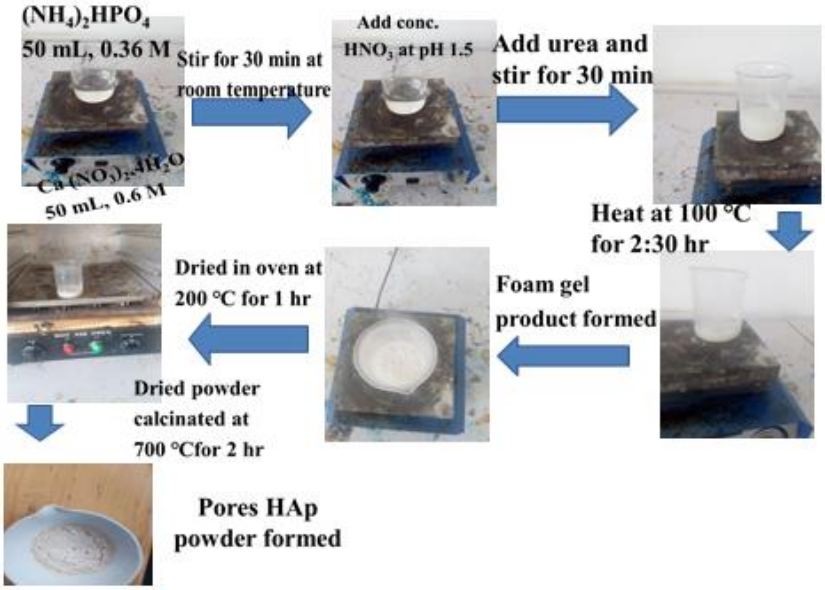

Figure 1: Experimental flow charts of synthesized HAp from urea optimized.

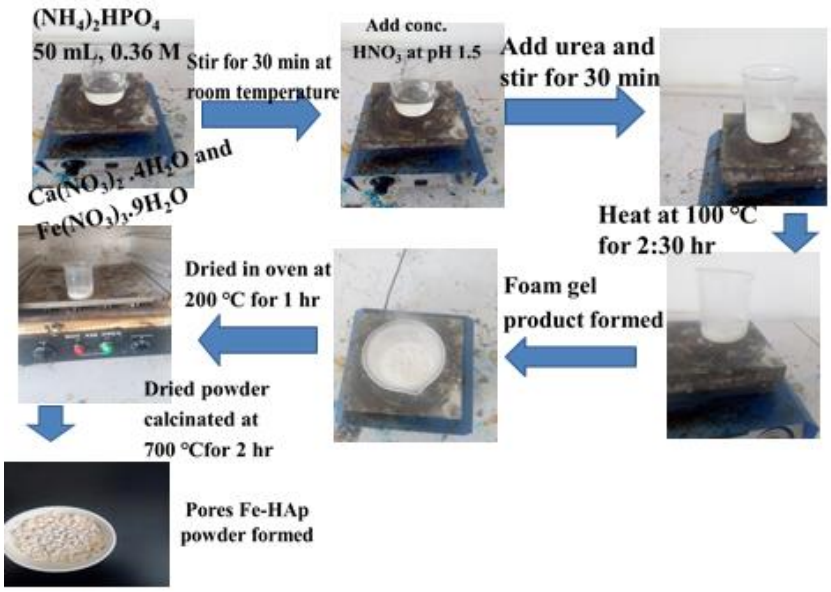

Figure 2: Experimental flow charts of synthesized Fe- HAp from iron mole optimized.